COHERENT PHOTOPRODUCTION OF ρ MESONS FROM DEUTERIUM

IRVING D. OVERMAN

STANFORD LINEAR ACCELERATOR CENTER

STANFORD UNIVERSITY

Stanford, California 94305

November 1971

ABSTRACT

Measurements of the forward differential cross section for the process $\gamma + d \rightarrow \rho^0 + d$ have been made at Stanford Linear Accelerator Center using a missing mass spectrometer. The recoil deuterons were detected by pulse height and time-of-flight.

Measurements were made at 6, 12, and 18 GeV and covered a momentum transfer range of $-0.15 > t > -1.4$ $(\text{GeV/c})^2$. The results were interpreted on the basis of the Glauber Model and found to be in excellent agreement. From this analysis values for both the total and differential cross section for the reaction $\rho^0 + N \rightarrow \rho^0 + N$ were extracted in rough agreement with the quark model.

The value of σ_T obtained in this experiment was used together with previous hydrogen photoproduction data and with total photoabsorption cross section measurements to determine $\gamma_\rho^2/4\pi$. The results of these two calculations are in disagreement well outside experimental errors and indicate the Vector Dominance Model does not describe all physical processes relating to photon-hadron interactions.

TABLE OF CONTENTS

LIST OF TABLES

LIST OF ILLUSTRATIONS

In recent years, Vector Dominance has become a fundamental concept in our understanding of the interaction of photons with hadrons. First formulated by J. J. Sakuri(42) in the early 1960's, Vector Dominance treats photons as completely equivalent to a superposition of the strongly interacting vector mesons ρ^o, ω, and ϕ. The most important member of this group is the ρ^o meson. The ρ^o meson is characterized by a very short lifetime (about 10^{-23} sec) and a correspondingly broad mass spectrum (about 130 MeV wide). The ρ has three charge states making it an isovector particle and has the same quantum numbers, as the photon (i.e., $J^{PC} = 1^{--}$). The Vector Dominance theory explained at least qualitatively a large mass of experimental phenomena. Firstly, it provided an interpretation of the pion form factor or photon-pion vertex function $F_\pi(q^2)$. Secondly, it roughly acounted for the decay processes:

$$\omega \rightarrow \pi^+ + \pi^- + \pi^o$$

$$\omega \rightarrow \pi^o + \gamma$$

$$\pi^o \rightarrow 2\gamma$$

$$\rho^o \rightarrow e^+ e^-, \mu^+ \mu^-$$

$$\omega^o \rightarrow e^+ e^-, \mu^+ \mu^-$$

$$\phi \rightarrow e^+ e^-, \mu^+ \mu^-$$

Thirdly, both the photoproduction of vector mesons, particularly ρ^0, and the photon-nucleon total cross sections could be quantitatively described(40).

To visualize this concept we consider an analogy to Quantum Electro-dynamics. In Quantum Electro-Dynamics the photon is thought of as making repeated virtual transitions to electron positron pairs in such a way that the mere presence of a massive (charged) body nearby to absorb the necessary momentum transfer will cause the electron positron pair to materialize as real particles. In a similar way the photon is thought of as making repeated virtual transitions to vector mesons states where an appropriately "charged" massive body in the neighborhood can cause the vector mesons to materialize in place of photons. In Vector Dominance the "charge" of the massive particle is equivalent to the strength of the vector meson coupling to it (see Fig. 1).

In more precise terms the electromagnetic current is related to the zeroth components of the isospin and hypercharge currents by means of the Current Field Identity:

$$j_\mu^{EM}(x) = - \sum_V \frac{m_V^2}{2\gamma_V} V_\mu(x) \qquad (1)$$

where $j_\mu^{EM}(x)$ is the electromagnetic source current and

$$\frac{e}{2} \frac{m_\rho^2}{\gamma_\rho}$$

FIG. 1: Vector dominance.

$V_\mu(x)$ is the vector meson current. The Feynman graph appropriate to the pion form factor is shown in Fig. 2 from which it can be shown:

$$F_\pi(q^2) = \frac{m_\rho^2}{m_\rho^2 - q^2} \; \frac{1}{2\gamma_\rho} \; g_{\rho\pi\pi} \tag{2}$$

where q is the four-momentum of the photon and $g_{\rho\pi\pi}$ is the strength of the ρ-π coupling.

This reduces for real photons to:

$$F_\pi(0) = 1 = \frac{g_{\rho\pi\pi}}{2\gamma_\rho} \quad \text{or} \quad \gamma_\rho = \frac{g_{\rho\pi\pi}}{2} \tag{3}$$

If we make the assumption that $g_{\rho\pi\pi}$ is a constant independent of q^2, we can calculate its value from the decay width of ρ^0 into two pions.

Similarly the first three decays listed above and shown in Fig. 3 yield the following relations:

$$\Gamma(\omega \to 3\pi) = \left(\frac{g_{\rho\pi\pi}^2}{16\pi}\right)\left(\frac{g_{\rho\pi\omega}^2}{4\pi}\right)\frac{(m_\omega - m_\pi)^4}{(m_\rho^2 - 4m_\pi^2)^2}\frac{m_\omega m_\pi^2}{\sqrt{27}} \tag{3.56}$$

$$\Gamma(\omega \to \pi^0\gamma) = \frac{\alpha}{96}\frac{g_{\rho\omega\pi}^2}{4\pi}\left(\frac{4\pi}{\gamma_\rho^2}\right)\frac{(m_\omega^2 - m_\pi^2)^3}{m_\omega^3} \tag{4}$$

$$\Gamma(\pi^0 \to 2\gamma) = \frac{\alpha^2}{576}\left(\frac{4\pi}{\gamma_\rho^2}\right)\left(\frac{4\pi}{\gamma_\omega^2}\right)\left(\frac{g_{\rho\omega\pi}^2}{4\pi}\right)m_\pi^3$$
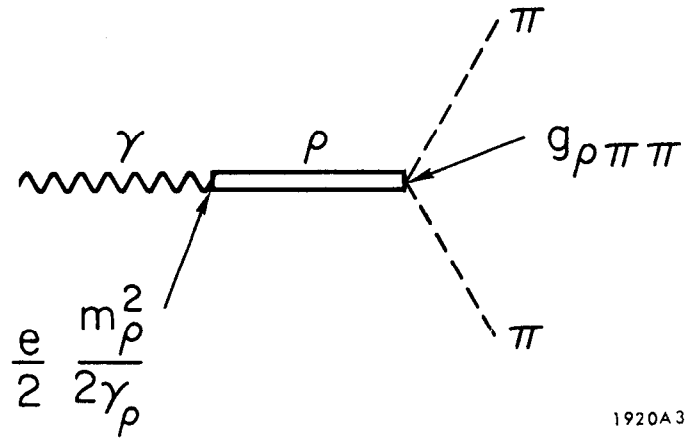
FIG. 2: Pion form factor.
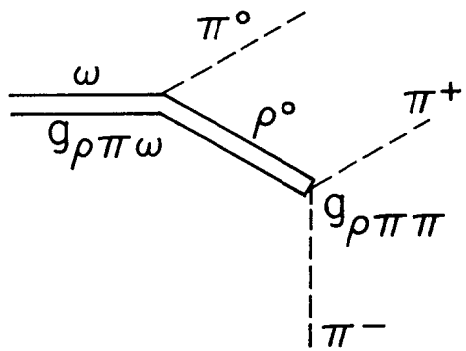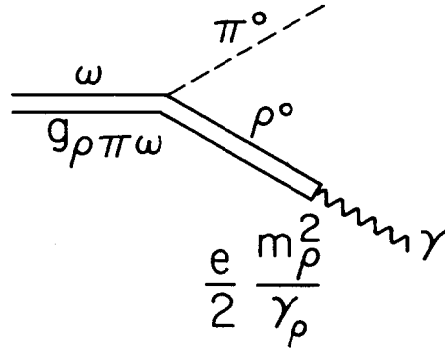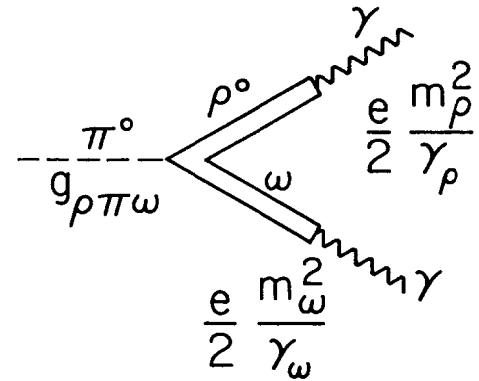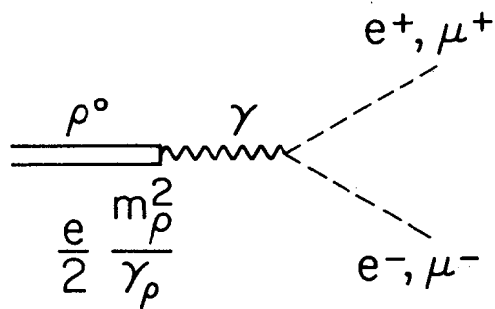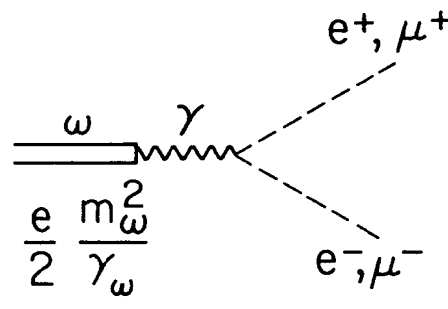
FIG. 3: Several decay processes.

1920B4

SU(3) and ω-φ mixing theory predicts the relative magnitudes of the three coupling constants γ_ρ^2, γ_ω^2, and γ_ϕ^2. This is done by noting that the ρ^0, ω, and ϕ are derived from an SU(3) octet plus a singlet. The ρ^0 and ω are composed of only non-strange quarks and the ϕ is composed of only strange quarks. The physical ω and ϕ are assumed to be:

$$|\omega> \equiv \cos\theta|\omega_1> - \sin\theta|\phi_8>$$

$$|\phi> \equiv \sin\theta|\omega_1> + \cos\theta|\phi_8>$$

where ϕ_8 is the I=0 member of the same SU(3) octet as the ρ, and the ω_1 constitutes an SU(3) singlet. Now if we assume further that the photon is the U spin singlet of an SU(3) octet and that the $V_{\pi\gamma}^0$ vertex is invariant under SU(3) transformations for all three of our vector mesons we conclude that:

$$\gamma_\rho : \gamma_\omega : \gamma_\phi = 1 : 3 : -3/\sqrt{2}$$

This result assumes exact SU(3) symmetry and is modified slightly when symmetry breaking and mass differences are taken into account. There are currently two ways to introduce this symmetry breaking. One is the so called "mass mixing" and the other "current mixing". The exact SU(3) symmetry gives the mixing angle as:

$$\cos\theta = \sqrt{2/3} \implies \theta \cong 35°$$

the "mass mixing" method gives $\theta \cong 39°$, while the current mixing gives $\theta \cong 28°$(33,43).

It is clearly of great interest to determine whether the Vector Dominance picture is exactly correct, approximately correct, or incorrect. A direct measure of the validity of the Vector Dominance concept is the extent to which all relevant processes are described in terms of unique coupling constants γ_V. The colliding beam process $e^+ e^- \to \rho^0 \to \pi^+ \pi^-$ can be used to investigate the q^2 dependence of γ_ρ^2 as can $\rho^0 \to e^+ e^-$ (see Fig. 4), but not to establish the uniqueness of γ_ρ^2 at $q^2 = 0$.

Photoproduction processes are related to corresponding vector meson elastic scattering processes as follows:

$$\frac{d\sigma}{dt}(\gamma A \to B) = \sum_V \frac{\alpha\pi}{\gamma_V^2} \frac{d\sigma}{dt} (V_{transverse} + A \to B) + \text{interference terms} \qquad (5)$$

In the case of ρ-photoproduction, the sum is often approximated by the single term involving the ρ itself (see Fig. 5). The ω and ϕ terms are neglected due to the relative weakness of their couplings. Furthermore, we can much more justifiably neglect terms corresponding to undiscovered vector mesons for the same reason. If we think in terms of vector dominance, ρ^0 photoproduction must

FIG. 4: Colliding beam ρ production.

Photon

$$\frac{e}{2}\frac{M_V^2}{\gamma_V}$$

Vector Meson

"Elastic Scattering"

Nucleon
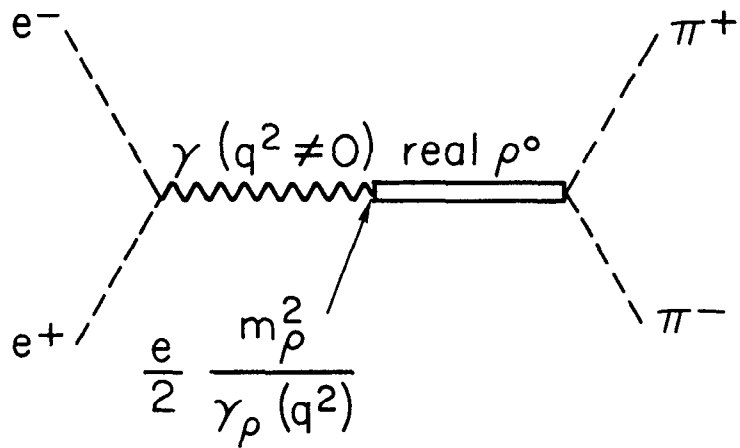
Nucleon
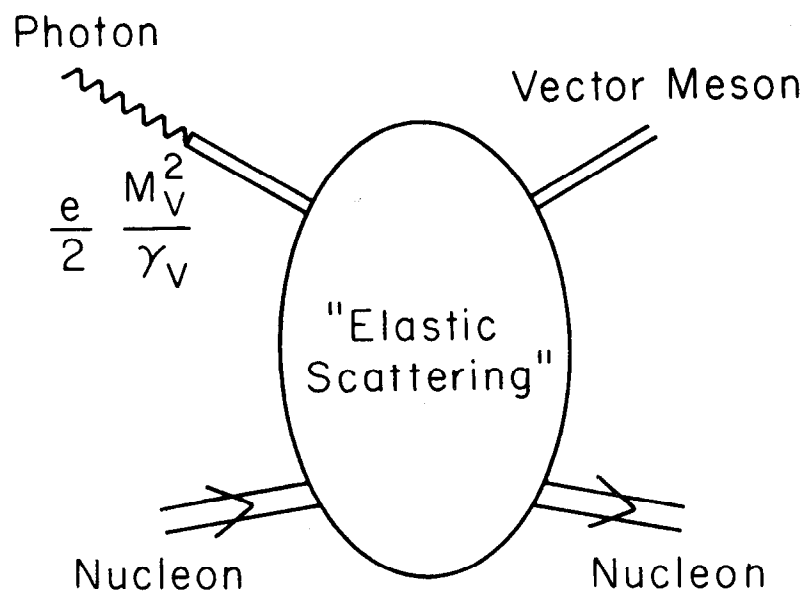
1920A2

FIG. 5: Photoproduction on hydrogen.

look like $\rho^{o}N$ elastic scattering which in turn should look like πN elastic scattering which is known to be diffractive. In fact, ρ^{o} photoproduction is diffractive and shows the characteristic forward peak $\propto e^{8t}$ (4). Even so there is still an ambiguity. If we now measure the photoproduction cross section the question arises: "How much is elastic scattering of ρ mesons and how much is $\rho - \gamma$ coupling?" That is, we have measured only the value of $\sigma_T^2 / \gamma_\rho^2$. Therefore, we have one equation and two unknowns. We could use the value deduced from other experiments but this would provide no check on the theory. Note that the photon-vector meson couplings are independent of the kinematics at the nucleon interaction. Thus in this view one measures the t-dependence of vector meson nucleons elastic scattering when measuring the t-dependence of photoproduction. If one can then measure the scale of the elastic scattering (σ_T) then the value of γ_ρ^2 can be inferred independently.

The straight forward way to measure σ_T would be to impinge a beam of ρ mesons on a hydrogen target. This idea is of course totally unfeasible as the energy of the ρ beam required for a mean flight path of 1cm would be 5×10^{14} GeV. At typical accelerator energies (15 GeV) a ρ must be produced and then scattered before it travels 30 fermis. The only way this can be accomplished is to

produce a ρ on one nucleon and scatter it from another
nucleon in the same atomic nucleus.

Recent experiments have used complex nuclei as targets
in just this manner(1,5,7,9,12,37). The idea here is to
produce the ρ^o on one nucleon and then observe the
absorption of the ρ's by the other nucleons in the nucleus.
The difficulty with these experiments is in knowing
precisely the average effective number of nucleons in the
path of the ρ^o after it is produced. The situation is
further complicated by the coherence of the photoproduction
process brought about by the tight binding of the nucleons.
For this reason the photoproduction cross section rises
with A faster than linearly even with the absorption
effects. Also there is the possibility of exciting the
nucleus out of the ground state into an ever increasing
number of excited states as A grows large. Thus, the
extraction of σ_T from these experiments requires an exact
understanding of nuclear physics. Furthermore, the phase
of the $\rho^o N$ scattering amplitude must be known in these
experiments in order to extrapolate the cross section to
t=0. As we recall, using the Vector Dominance concept the
phase of the $\rho^o N$ scattering amplitude should be the same as
the phase of proton Compton scattering $\gamma + p \rightarrow \gamma + p$ (see
Fig. 6). This follows since the $\gamma - \rho^o$ coupling is real.
However certain possible processes such as in Fig. 7 weaken

-12-
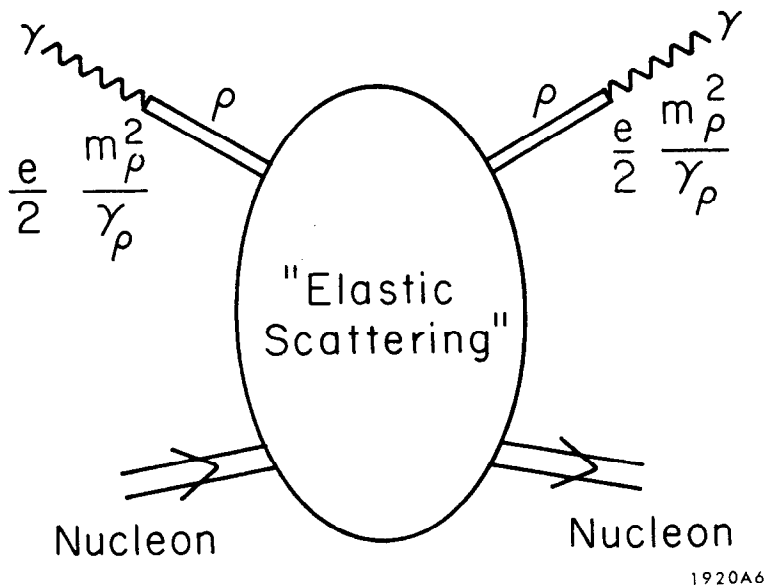
FIG. 6: Compton scattering on protons.
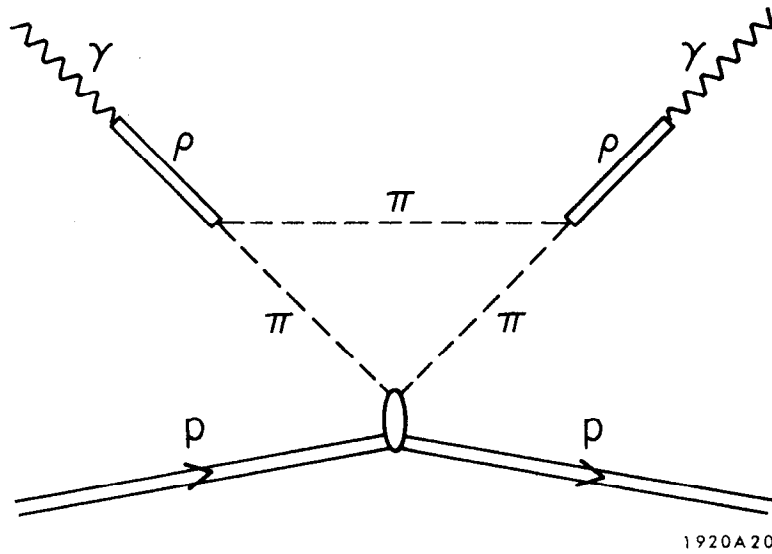
FIG. 7: Phase changing diagram.

1920A20

this conclusion somewhat. Measurement of the real part of the Compton amplitude is extremely difficult. The total cross section is quite well known however and dispersion relations can be used to calculate the real part to good accuracy(15). For a detailed review of photoproduction on complex nuclei see Harold Ogren's Thesis (38).

B. H. Wiik observed that we can avoid most of this confusion by studying the reaction $\gamma + d \rightarrow \rho^O + d$ where the recoil deuteron is observed and identified. Since deuterium has no bound excited states, the final state is unambiguously determined, and furthermore, the ground state wave functions for deuterium are well known. Since the deuteron is an isoscalar particle, the amplitude for this process can contain no contributions from the isoscalar part of the photon, and hence the ω and ϕ terms as well as the interference terms in Eq. 5 are rigorously zero. Such would not be the case for the process $\gamma + p \rightarrow \rho^O + p$ since the proton has non-zero isospin.

A particularly elegant description of this process is provided by the multiple diffraction theory of Glauber(24,26). The Glauber theory allows us to extract the differential cross section for $\rho^O + N \rightarrow \rho^O + N$ as well as the total cross section σ_T. Furthermore, analysis of previous experiments using this theory have shown it to be quite reliable in the high energy, low momentum transfer

region(21,25).

The Glauber theory assumes that a high energy particle is incident on a nucleus such that its wave length is short compared to the inter-nucleon-distance. Each scattering of the incident particle is assumed to be diffractive and therefore involves many partial waves with high angular momenta. The momentum transfer given to each nucleon is further assumed to be small enough so that no nucleon becomes relativistic. In analogy to optics then, the phase shifts from each scattering add to give the total phase shift associated with each partial wave.

Applying the additivity of phase shifts and isospin invariance leads us to express the amplitude for the process $\gamma + d \rightarrow \rho^{0} + d$ as:

(6)

$$F(\vec{q},\vec{r}) = 2 \, f_p(\vec{q}) \, e^{i\vec{q} \cdot \vec{r}/2} + \frac{i}{2\pi k} \int_{q_{min}}^{\infty} e^{i\vec{q} \cdot \vec{r}} \, f_p(\tfrac{1}{2}\vec{q} - \vec{q}') f_e(\tfrac{1}{2}\vec{q} + \vec{q}') d^2_{q'},$$

where $f_p(\vec{q})$ is the amplitude for $\gamma + N \rightarrow \rho^{0} + N$, $f_e(\vec{q})$ is the amplitude for $\rho^{0} + N \rightarrow \rho^{0} + N$, $q \equiv k-k'$, and $q_{min} = m_\rho^2/4k$.

The first term in Eq. 6 is due to photoproduction on a single nucleon where the other nucleon is a spectator. The second term corresponds to photoproduction on one nucleon followed by elastic scattering on the other (see Fig. 8). In principle, there are any number of terms corresponding

(a)

(b)
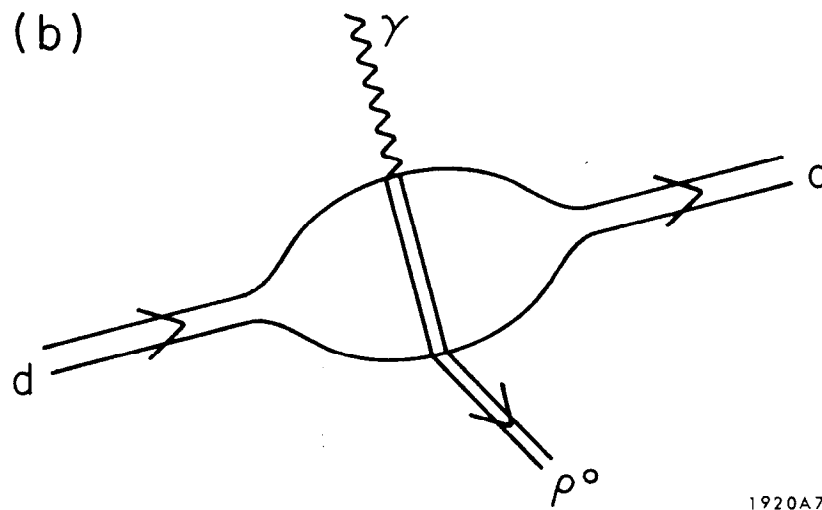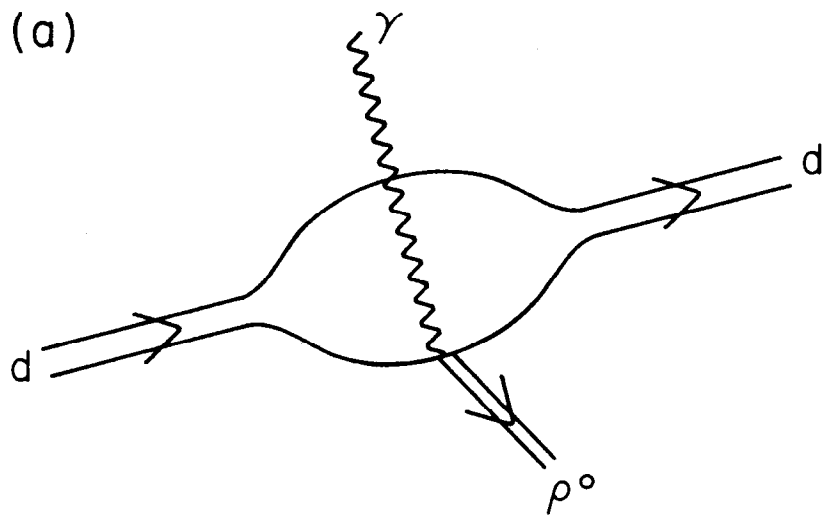
FIG. 8: Photoproduction on deuterium:

    a) single scattering
    b) double scattering

1920A7

to $\gamma + N \rightarrow X + N$ followed by $X + N \rightarrow \rho^0 + N$. These terms will be neglected for the time being, becoming a potential source of error. Evaluating this amplitude between initial and final states of the deuteron we conclude that:

$$\frac{d\sigma}{dt}(t)_{\gamma d \rightarrow \rho d} = 4 \frac{d\sigma}{dt}(t)_{\gamma \rho} \left[S_0^2(q/2) + S_2^2(q/2) \right]$$

$$- \frac{2}{\pi^{3/2}(1+a^2)^{1/2}} \left[K_0 S_0(q/2) + \frac{1}{4} K_2 S_2(q/2) \right] \left[\frac{d\sigma}{dt}_{\gamma \rho}(t/4) \frac{d\sigma}{dt}_{\rho N}(t/4) \right]^{1/2}$$

$$+ \frac{1}{4\pi^3} \left(K_0^2 + \frac{1}{4} K_2^2 \right) \frac{d\sigma}{dt}_{\gamma \rho}(t/4) \frac{d\sigma}{dt}_{\rho N}(t/4) \tag{7}$$

where a is the ratio of real-to-imaginary parts of f_e,

$$q = \left[t + \frac{t^2}{4M_d} \right]^{1/2} \tag{8}$$

is the three momentum transfer, S_0 and S_2 are the static and quadrupole form factors of the deuteron respectively, and K_0 and K_2 are well defined integrals given by:

$$K_0 f_p(q/2) f_e(q/2) = \int_{m_\rho^2/4k}^{2k} S_0(\vec{q}\,') f_p(\vec{q}/2 - \vec{q}\,') f_e(\vec{q}/2 + \vec{q}\,') d^2\vec{q}\,'$$

$$\tag{9}$$

$$K_2 f_p(q/2) f_e(q/2) = \int_{m_\rho^2/4k}^{2k} S_2(\vec{q}\,') f_p(\vec{q}/2 - \vec{q}\,') f_e(\vec{q}/2 + \vec{q}\,') d^2\vec{q}\,'$$

-18-

$d\sigma/dt_{\gamma\rho}$ is the cross section for photoproduction on hydrogen while $d\sigma/dt_{\rho N}$ is the ρ nucleon elastic scattering cross section. The form factors are defined as follows:

$$S_0(q) \equiv \int_0^\infty \left[u^2(r) + w^2(r) \right] \; j_0(qr)dr$$

$$S_2(q) \equiv \int_0^\infty \left[u(r) - \frac{w(r)}{\sqrt{8}} \right] 2w(r) \; j_2(qr)dr \qquad (10)$$

where u(r) and w(r) are the deuteron S and D ground state wave functions respectively.

The integrals represent the cohesive properties of the deuteron in that they formalize the deuteron's ability to remain bound given a momentum transfer difference of $2\vec{q}'$ between the two nucleons summed over all possible cases. The single scattering terms in Eq. 9 contains no such integral since $\vec{q}' = \vec{q}$ by definition. The deuteron form factors are shown in Fig. 9. These were computed using the wave functions of Hamada and Johnson(30). All reasonable deuteron wave functions yield form factors which are in good agreement out to q of 0.8(GeV/c). If we assume that the amplitudes $f_p(q)$ and $f_e(q)$ are given by an exponential in q^2 appropriate to diffraction scattering we note that the first or single scattering term in Eq. 9 falls extremely rapidly with |t| whereas the last or double
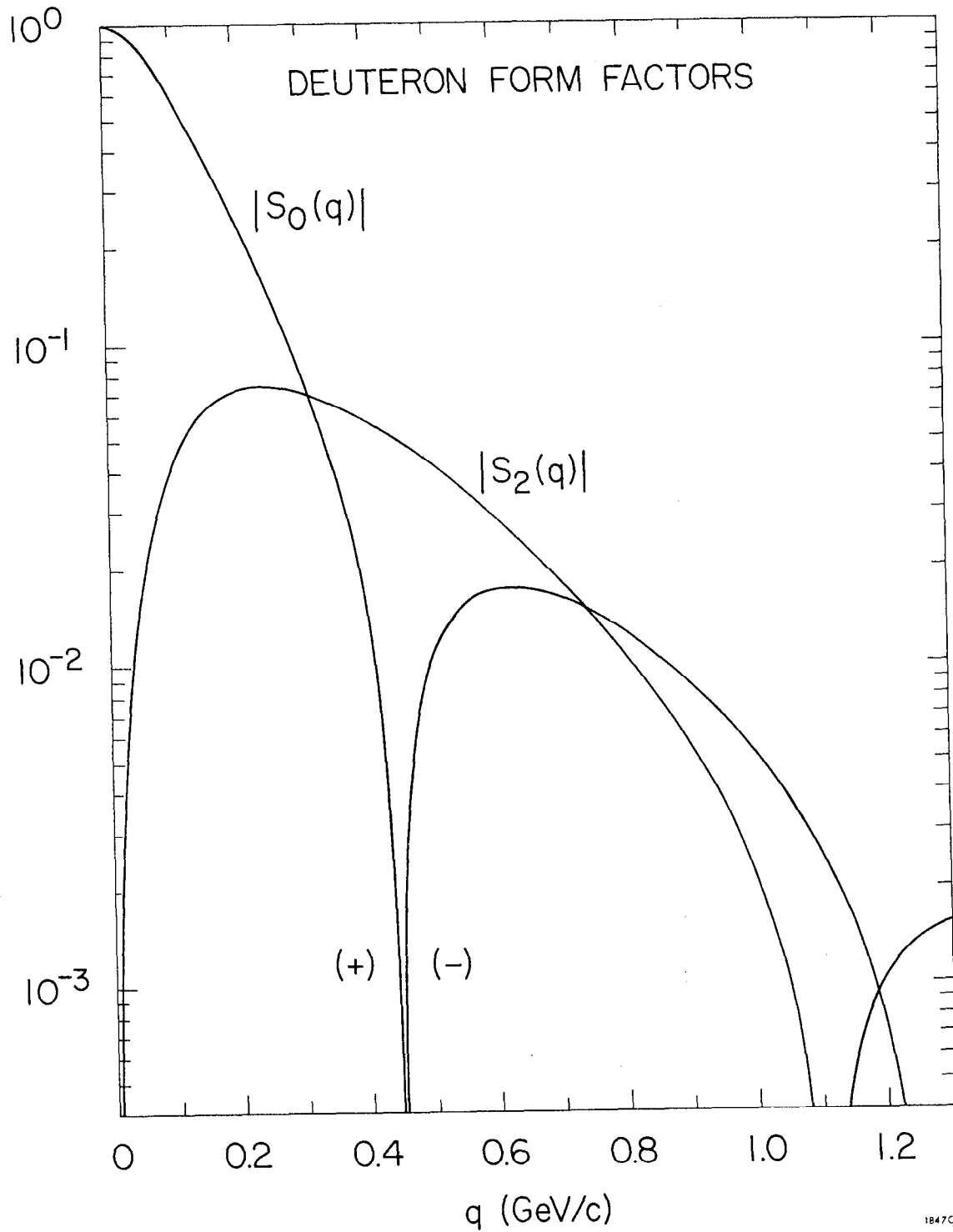
FIG. 9: Deuteron form factors.

scattering term falls relatively slowly. The interference term between single and double scattering only becomes important in the region near t = -0.3 where the other two terms are comparable in size. Thus we have a region near t = 0 where the cross section is $\propto \sigma_T^2/\gamma_p^2$, followed by a region of confusion around t = -0.3 and finally a region where the cross section is $\propto \sigma_T^4/\gamma_\rho^2$. Therefore one could extract σ_T^2 and $4\pi/\gamma_\rho^2$ using data from $\gamma + d \rightarrow \rho^0 + d$ alone. Alternatively one could compare $\gamma + d \rightarrow \rho^0 + d$ data with $\gamma + p \rightarrow \rho^0 + p$ data and extract the $\rho^0 + N \rightarrow \rho^0 + N$ cross section yielding a value for σ_T which then can be used in conjunction with the $\gamma + p \rightarrow \rho^0 + p$ data again to compute $4\pi/\gamma_\rho^2$.

In order to perform this experiment it is necessary to isolate the process $\gamma + d \rightarrow \rho^0 + d$ and require that the deuteron not break up. Furthermore, the level of precision required is around 10% in the deuteron cross section and about 1% in t. Since the cross section in the "double-scattering" region is a few nanobarns/(GeV/c)^2 an intense beam and a detection system with a large acceptance is required. Due to much larger backgrounds the detection system must also be capable of operating at a high rate with good rejection. A previous experiment(4,32) had been done at Stanford Linear Accelerator Center measuring differential cross section for $\gamma + p \rightarrow \rho^0 + p$ in the

-21-

forward direction. It was clear that if one could do the $\gamma + d \rightarrow \rho^0 + d$ experiment using the same apparatus, many of the systematic errors in the two experiments would cancel allowing a much more reliable measurement of σ_T. To perform the experiment we used the SLAC 1.6 GeV/c spectrometer to detect the deuterons identifying them by pulse-height in scintillation counters and time-of-flight. The experiment was done at 6, 12, and 18 GeV over a range of momentum transfer $-0.15 \geqslant t \geqslant -1.4 (GeV/c)^2$. The cross sections were analyzed using the Glauber theory which gave excellent fits to the data and yielded precise values for σ_T. $\gamma_\rho^2/4\pi$ was then calculated to be about .65 in agreement with recent analyses of photoproduction experiments done on heavy nuclei. If we however take our value of $\sigma_{\rho N}$ we can extract an independent determination of $\gamma_\rho^2/4\pi = .47$ at 12 GeV. This result is in contradiction to our value based on photoproduction and indicates that the electromagnetic current is not saturated by the known Vector mesons.

The extracted $\rho^0 N$ differential cross sections were found to be in reasonable agreement with the quark model prediction:

$$\left[\frac{d\sigma}{dt}(\rho^0 + N \rightarrow \rho^0 + N)\right]^{1/2} = \frac{1}{2}\left[\frac{d\sigma}{dt}(\pi^+ + p \rightarrow \pi^+ + p)\right]^{1/2} + \frac{1}{2}\left[\frac{d\sigma}{dt}(\pi^- + p \rightarrow \pi^- + p)\right]^{1/2}$$

(11)

assuming equal real parts.

II. EXPERIMENTAL METHOD

The experiment was done at Stanford Linear Accelerator using the SLAC high energy bremsstrahlung beam and the 1.6 GeV/c magnetic focussing spectrometer. The apparatus is shown in Fig. 10. The beam was prepared by directing the SLAC high power electron beam onto a metal radiator, sweeping the electrons into a dump, and allowing the produced bremsstrahlung beam to pass through several collimators and Cerenkov monitor into a deuterium target. The photons were then collected in a secondary emission quantameter (SEQ) to provide a measure of the total beam energy. The electron beam was modulated at the injector with a pulser especially built for SLAC by EGG to provide bunches of electrons about 5nsec (FWHM) wide and separated by 40-100 nsec according to the frequency of the trigger signal. This means that the events of interest would occur in bursts lasting approximately 5nsec in the center of the target.

The spectrometer used to detect the deuterons is shown in Fig. 11. It consists of a vertical, 100" central radius, 90° bend magnet which focuses both momentum and angle of charged particles recoiling from the target, a transport mechanism to allow rotation about the target in the horizontal plane, appropriate aperture defining
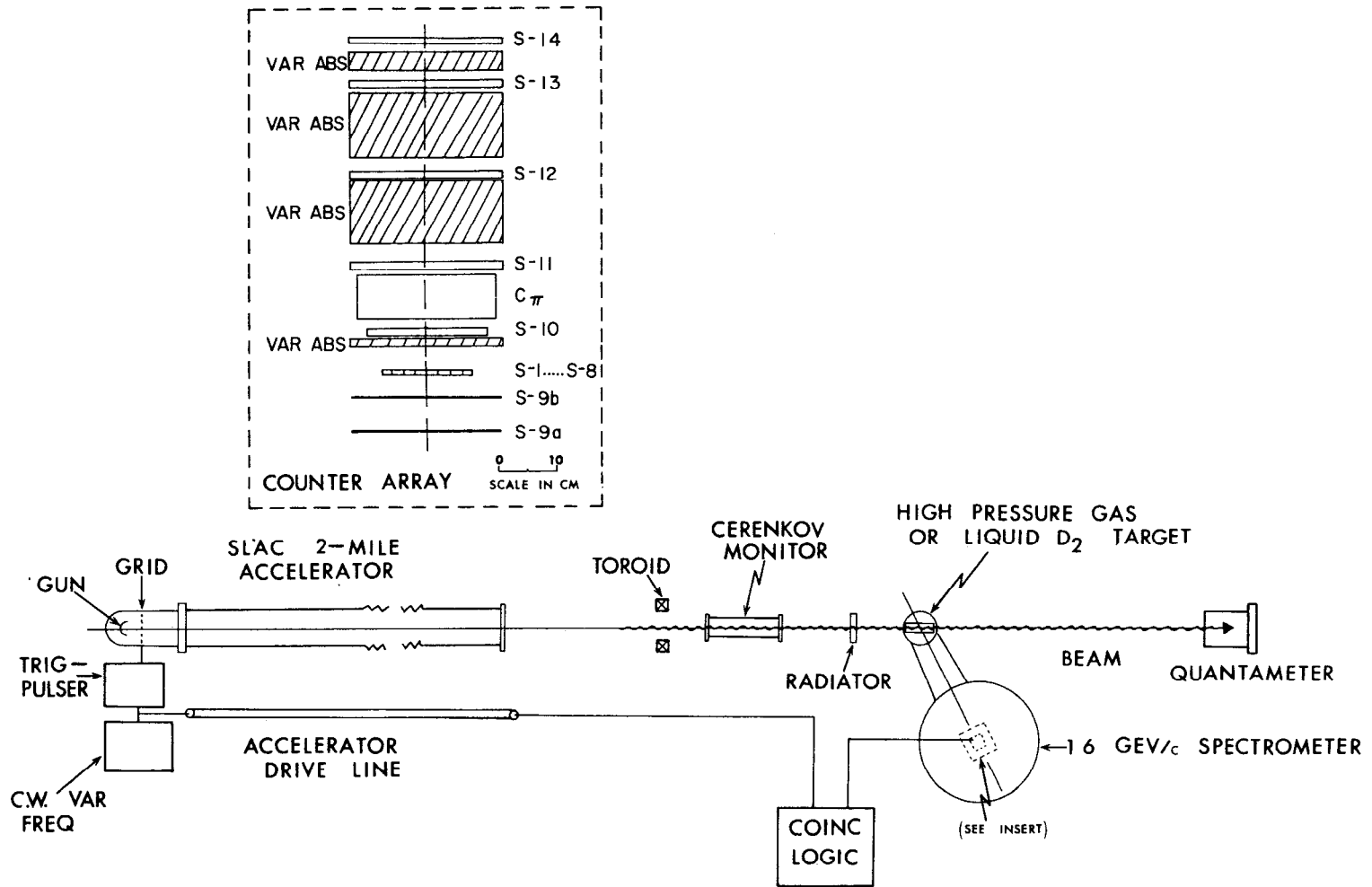
FIG. 10: Experimental arrangement.

TOP VIEW

COUNTER CAVE·

100-INCH
MAGNET

VACUUM
CHAMBER

REMOVEABLE
SHIELDING BLOCK

MOVEABLE
LEAD DOORS

CONCRETE SHIELDING

SLAC 1.6 GeV c SPECTROMETER

COUNTER CAVE

MOVEABLE
LEAD DOORS

FOCAL
PLANE

CONCRETE
SHIELDING
BLOCKS

VACUUM
CHAMBER

COILS

RETRACTABLE
NMR PROBE

100 INCH 90°
BEND MAGNET

VERTICAL AND
HORIZONTAL
ENTRANCE MASK

FOCAL PLANE

NMR
OSCILLATOR

TARGET TABLE

PIVOT

SUPPORT
STRUCTURE

0   1'   2'
SCALE

1920A17
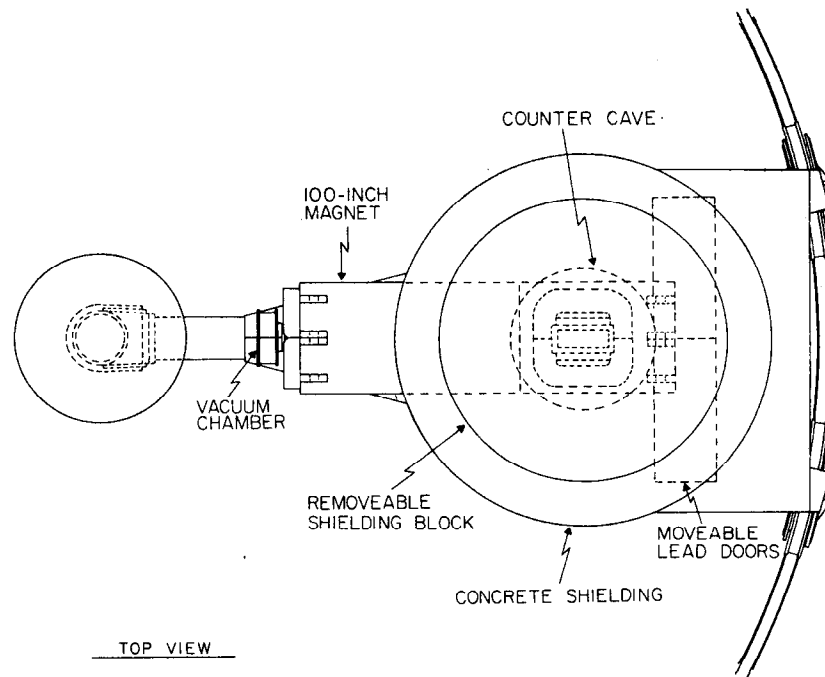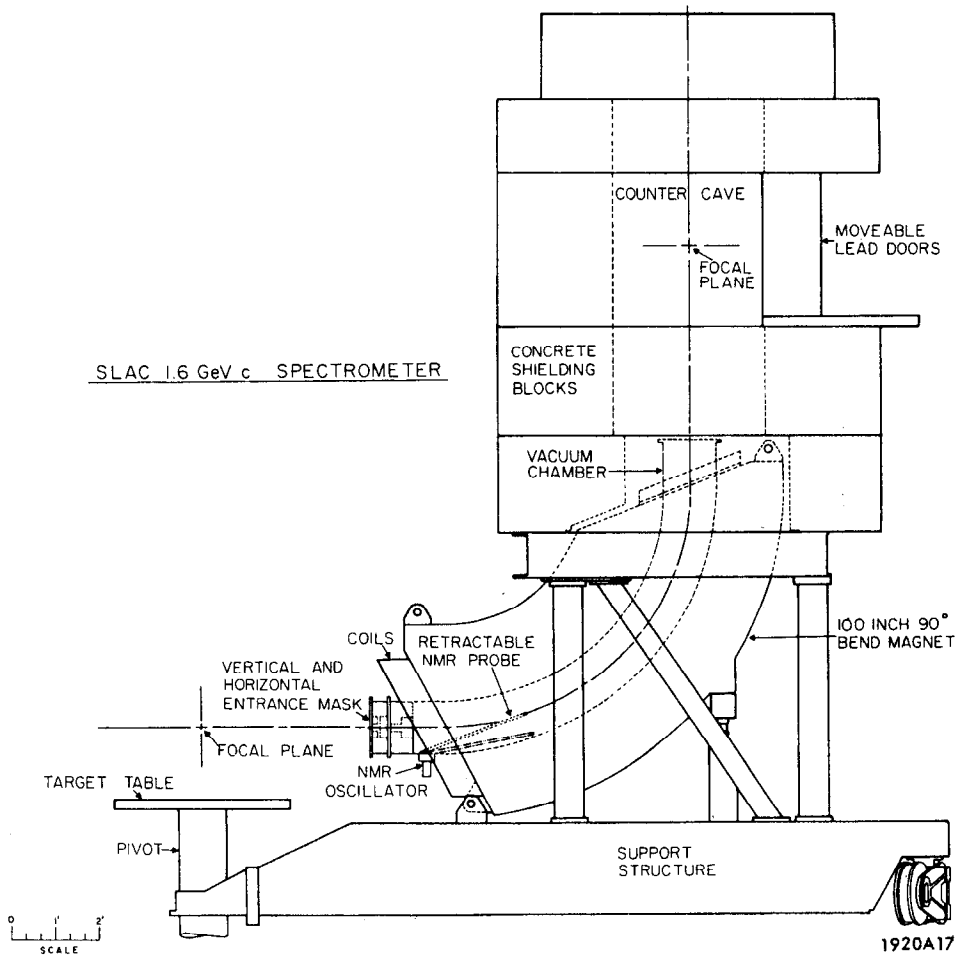
FIG. 11: SLAC 1.6 Gev/c spectrometer.

-25-

collimators, and a shielded room for installing detectors. The slanted pole faces of the magnet iron cause the focal planes for momentum and angle to coincide. Second-order corrections and rotation of the focal plane so that it is horizontal are accomplished by three beta lenses inside the magnet. The net result is that at 254cm(100") above the exit of the central ray we have a simple plane where we can plot p and θ. In that plane we have a momentum dispersion of

$$p \frac{\partial x}{\partial p} = 4.19 \, cm/\%$$

which varies across the useful aperture of about 6% by

$$p^2 \frac{\partial x^2}{\partial p^2} = 4.95 \times 10^{-2} \, cm/(\%)^2$$

having an intrinsic momentum resolution of ± 0.08%. Also in that plane we have an angular dispersion of

$$\frac{\partial y}{\partial \theta} = 0.823 \, cm/mr$$

which varies across the useful aperture of about 17mrad by

$$\frac{\partial y^2}{\partial \theta^2} = 2.5 \times 10^{-4} \, cm/(mr)^2 \, , \, p \frac{\partial y^2}{\partial \phi \partial p} = 1.24 \times 10^{-2} \, cm/mr/\%$$

-26-

having an intrinsic angular resolution of ± 0.37mrad. Table 4 lists other relevant magnet parameters.

The counter system consisting of a range telescope, a rotatable hodoscope, and a lucite threshold Cerenkov counter is shown in the insert to Fig. 10.

There are essentially four kinds of particles which reach the shielded cave in significant numbers. These are pions, protons, deuterons and K^+'s. Positrons are not prevented from entering the apparatus, but are not produced in significant numbers at large angles. First, we noted that the deuterons are far from minimum ionizing throughout the range of momenta of interest; thus their pulse heights in scintillation counters are larger than any of the other particles. Therefore we biased the electronics to reject the weaker pulse resulting from π's and protons as much as we could without losing deuterons. This was very effective against pions but not satisfactory for protons. Next we noted that the range of the deuterons is quite short at these momenta. Therefore we could use range to veto protons and pions. However since the deuteron may break up with a high probability, this method is extremely dangerous and must be done carefully. Thirdly, since the events could be restricted to a 5nsec time interval in the target, we could descriminate between deuterons and other particles on the basis of flight time through the spectrometer.

Fig. 12(a) shows a typical time-of-flight spectrum obtained using only pulse-height rejections at $t = -0.5(GeV/c)^2$. The width of the window shown there was about 20nsec and provided an unambiguous deuteron signal.

For this experiment, it was sufficient to identify the recoil deuteron and measure the magnitude and direction of its momentum. This fortunate consequence of kinematics can be seen as follows. If we defined the laboratory four-momentum of the incoming photon as $k_\mu = (\vec{k}, E_\gamma)$, the target particle as $M_\mu = (\vec{0}, m_d)$, the recoil dueteron as $p_\mu = (\vec{p}, E_d)$, and the produced whatever as $X_\mu = (\vec{X}, E_x)$ we have the following relations:

$$S \equiv (k_\mu + M_\mu)(k^\mu + M^\mu) = m_d(2E_\gamma + m_d)$$

$$t \equiv (p_\mu - M_\mu)(p^\mu - M^\mu) = 2m_d(E_d - m_d) \text{ or } -2m_d T_d \qquad (12)$$

$$m_x^2 \equiv (k_\mu + M_\mu - P_\mu)(k^\mu + M^\mu - p^\mu) = 2E_\gamma (P\cos\theta_d - T_d) + t$$

It is clear from Eq. 12 that there are only four kinematic variables to consider: E_γ, P, θ, and M_x. The first two of equation 12 supply the relevant Mandelstam invariants while the third defines a hypersurface upon
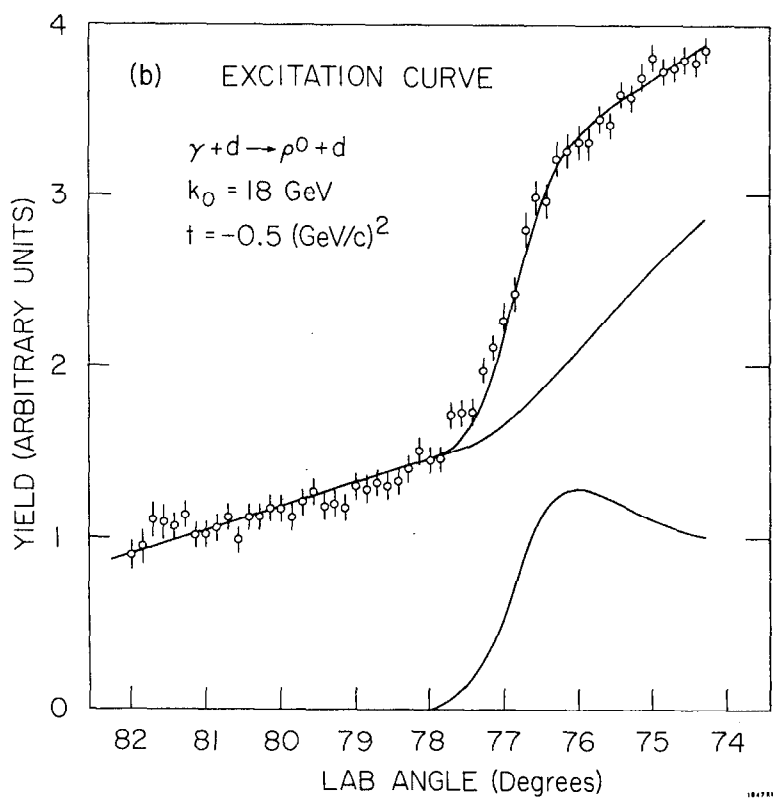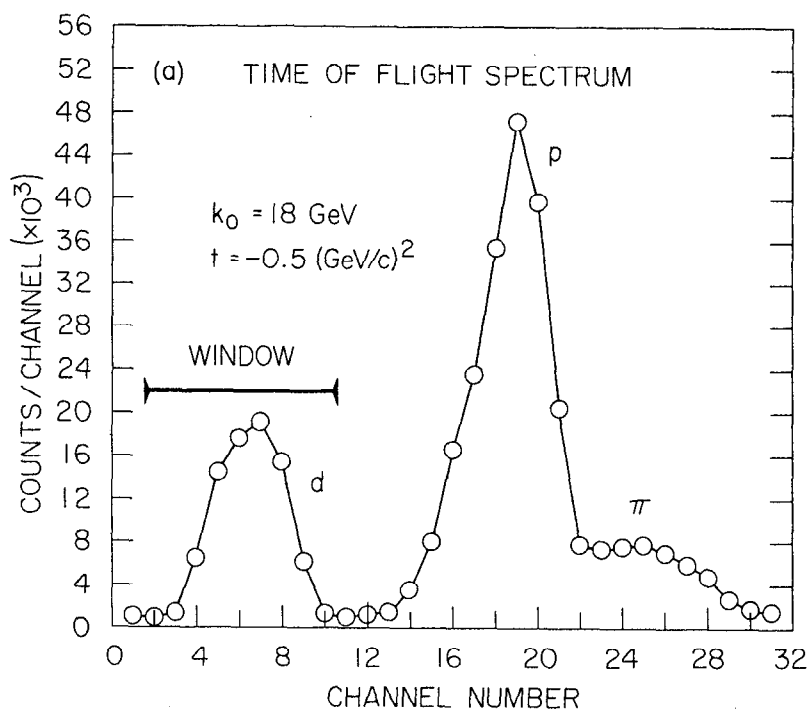
FIG. 12: a) Time-of-flight spectrum.
b) Resultant yield curve.

which real events must occur. Therefore one may specify any three of said variables to define the event completely. Suppose now we project this hypersurface onto a hyperplane of constant E_γ. Then we have a two dimensional surface in three dimensions (M_x, P, θ). Fig. 13 shows a contour map of such a surface projected out at E_γ = 12 GeV. Alternatively one can project onto a constant M_x hyperplane and draw another contour map. The result is Fig. 14. The spectrometer acceptance becomes a small area which can be positioned anywhere on these surface projections. Each point corresponds to the mass of the unobserved particle given the photon energy as in Fig. 13 or to photon energy given the "missing" mass as in Fig. 14. Note that over almost the entire momentum range that both sets of contours form essentially straight lines and would show no noticable curvature over the aperture of the spectrometer. Therefore one may merely place a "missing mass" hodoscope in the focal plane oriented along the contour lines to differentiate unobserved particles of different masses. Alternatively if the mass of the unobserved particle is known, the same hodoscope could be used to differentiate photons in the primary beam of different energies. Unfortunately in this experiment neither the beam energy nor the ρ^0 mass is constant. Therefore one obtains a rate in such a hodoscope given by:
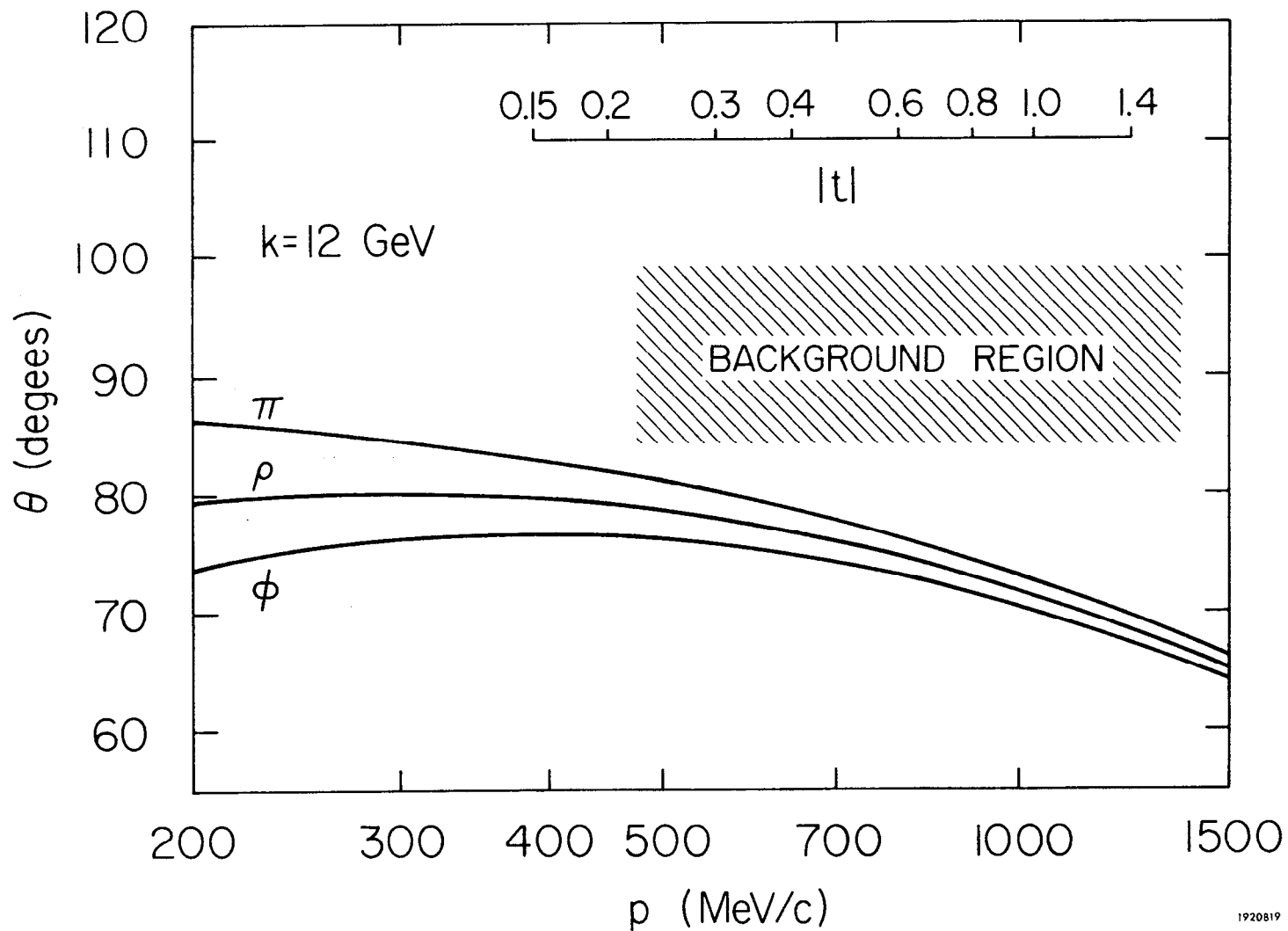
FIG. 13: Contour map of p,θ plane at constant E_γ.
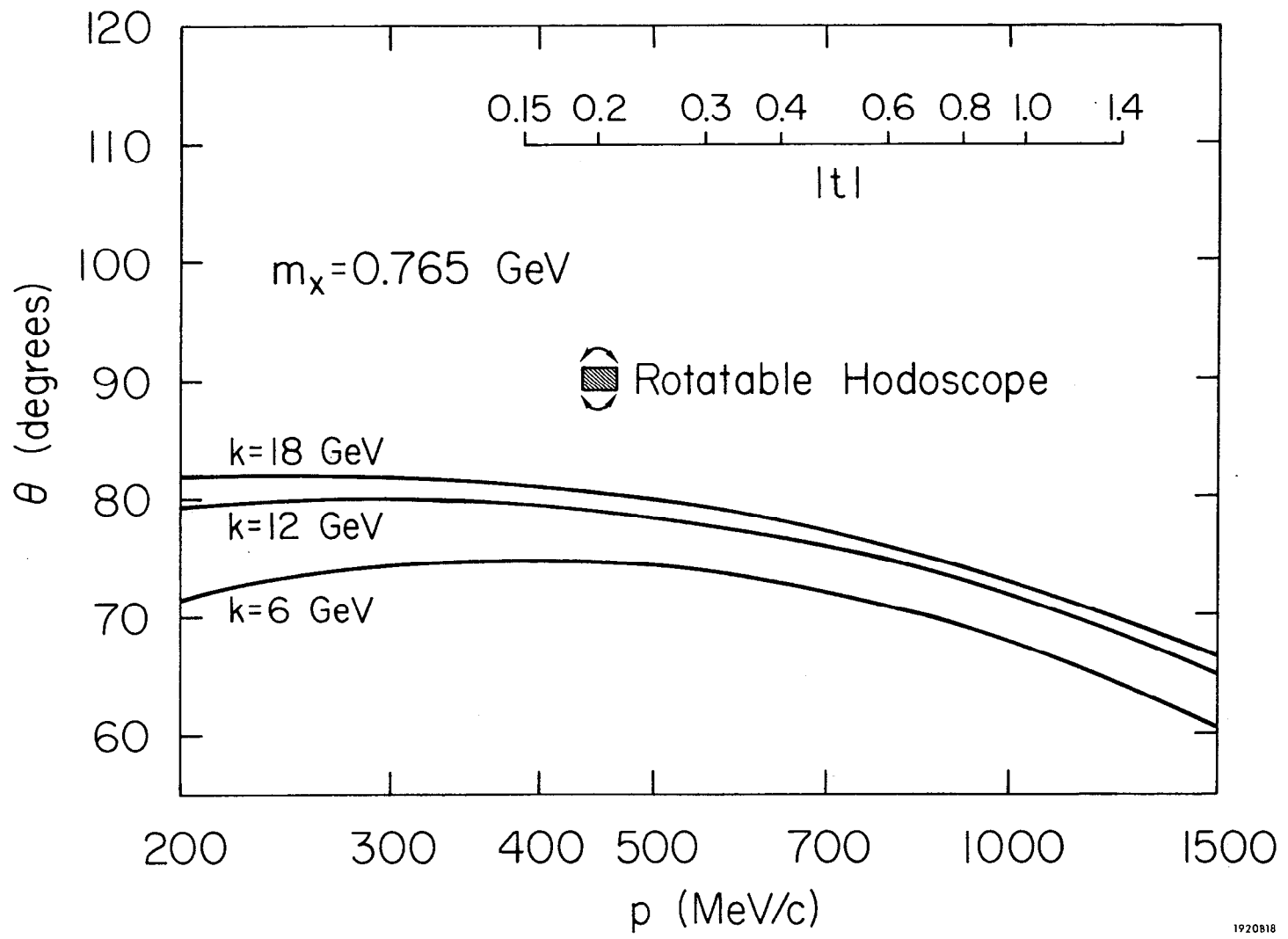
FIG. 14: Contour map of p, θ plane at constant M_x.

$$R(p,\theta) = \frac{dW_\gamma}{d\underline{t}} \frac{N_T}{E_o} \int\limits_0^{E_o} dk \frac{\partial(t,k)}{\partial(p,\theta)} \frac{dn(k)}{dk} p \frac{\Delta\phi\Delta\theta}{4\pi} \frac{\Delta p}{p} \int\limits_0^\infty dm \frac{\partial^2\sigma}{\partial t\partial m} \quad \times$$

(13)

$$\delta(m_x^2 - t - 2E_\gamma(p\cos\theta - T_d))$$

where

dW$_\gamma$/d$\underline{t}$ is the beam power

E_o is the end-point or Electron energy

N_T is the number of target deuterons per unit area

$$\frac{\partial(t,k)}{\partial(p,\theta)} = \frac{2M_d kp^2\sin\theta}{(p\cos\theta - T_d)E_d}$$

dn(k)/dk is the photon energy distribution normalized

so that

$$\int\limits_0^{E_o} k \frac{dn(k)}{dk} dk = 1$$

$\Delta\phi$ is the vertical angular acceptance of the spectrometer defined by the upper and lower jaws at the entrance to the magnet. $\Delta\theta\Delta P/P$ is an invariant acceptance defined by the area of the hodoscope counter in the focal plane.

$\frac{\partial^2\sigma}{\partial t\partial m} = \frac{d\sigma}{dt}D(m)$ where D(m) is the ρ^o mass distribution such that

$$\int_0^\infty D(m) \, dm = 1$$

The δ function is the kinematic constraint imposed by the last of equations 12. If we note that

$$N_T = \frac{\lambda L}{\sin\theta \, M_d}$$

where λ is the density of the target and $L/\sin\theta$ is the effective target length defined by the left and right jaws (set a distance L apart) at the entrance to the magnet, we conclude that:

$$R(p,\theta) = \frac{dW_\gamma}{dt} \frac{\lambda L}{E_0} \frac{\Delta\phi}{2\pi} \frac{p^3 m_d}{E_d} \frac{\Delta\theta\Delta p}{p} \int_0^{E_0} dk \, k \frac{dn(k)}{dk} \frac{1}{(p\cos\theta - T_d)} D(M_x(k,\theta,p)) \frac{d\sigma}{dt}(p,k)$$

(14)

where $m_x(k,\theta,p)$ is given by the δ function.

If the missing particle were a π^0 instead of a ρ^0, and we swept across the production threshold in the p, θ plane perpendicular to the contour lines we would see the shape of the bremsstrahlung spectrum traced out by the rate. Alternatively, if we were using a monochromatic beam we would see the ρ^0 mass distribution traced out. Both curves would be distorted however, since the effective spectrometer acceptance in the s,t plane shrinks with increasing mass or with decreasing photon energy due to the

Jacobian transformation involved. Also if the cross section varies with s, the curves will be further distorted. For this reason the s dependence of the cross section as well as the shape of ρ^0 mass distribution must be chosen as inputs to the analysis.

Fig. 12(b) shows a typical excitation curve obtained in this manner along with a fit calculated from Eq. 14. To obtain this curve, the spectrometer current was fixed, the rotatable hodoscope was aligned with the kinematic contour lines, and the azimuthal angle was stepped in units(bins) corresponding to the projected width of a hodoscope counter. The precise value of the magnetic field was measured by means of a retractable Nuclear Magnetic Resonance probe fitted to the inside of the spectrometer vacuum chamber. The regulation of the magnet current was good to ≤ .5% over each entire sweep. The angle was stepped in such a fashion that the counts for any given angle bin were accumulated by adding several runs each having a different hodoscope counter in the correct position for that bin. This procedure minimized errors due to non-uniform illumination of the hodoscope by background.

The photon beam was monitored simultaneously by a secondary emission quantameter(2) and a helium Cerenkov monitor(22). The Cerenkov monitor was used as an intermediate standard to calibrate the SEQ against a silver

calorimeter. The absolute systematic uncertainty in our calibrations was around 1%. The long term reproducibility of the SEQ was also around 1% leading to an overall uncertainty of 2% in monitor normalization. The electron beam was also monitored continuously by a toroid placed prior to the photon radiator. The ratios of these monitors were watched carefully for telltale signs of steering changes.

At 6 GeV incident energy it was necessary to allow the electron beam to pass through a thick radiator just prior to passing through the target. This was done in order to maximize the intensity of the produced bremsstrahlung beam. Due to the thickness of the radiator, the target was placed as close as possible in order not to allow the divergent photon beam to strike the walls of the deuterium container. Since the high power electron beam was allowed to pass through the target we could not use the SEQ to monitor the beam. Therefore we placed a second toroid just prior to the thick radiator to measure the beam intensity. The resulting photon spectrum and electroproduction corrections to our results were calculated by standard methods from Quantum Electrodynamics(14).

Two targets were used (see Figures 15 and 16). A condensation liquid D_2 target was used for $|t|$ above 0.3, while a pressurized gas target(2,3) was used at $|t| = 0.3$ and
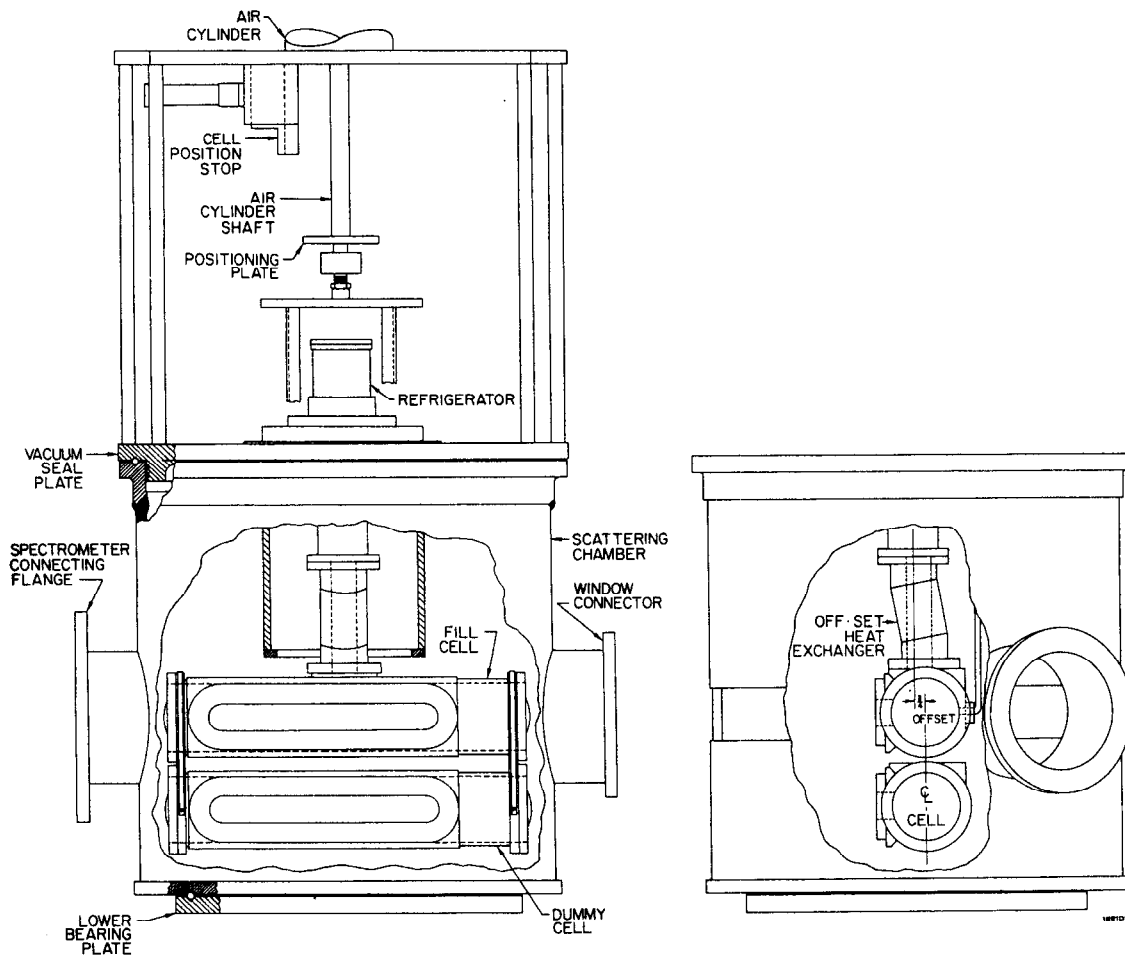
FIG. 15: High pressure gas target.

SLAC HIGH POWER
HYDROGEN
TARGET

VENT→

TO GASEOUS
H₂ SUPPLY

TO LIQUID
H₂ SUPPLY

RESERVOIR

ALUMINIZED MYLAR
THERMAL
INSULATION

LIQUID
HYDROGEN

CELL

BEAM→

DUMMY CELL

THIN WINDOW

SCATTERING
CHAMBER

0   3   6
SCALE IN INCHES
1920A15
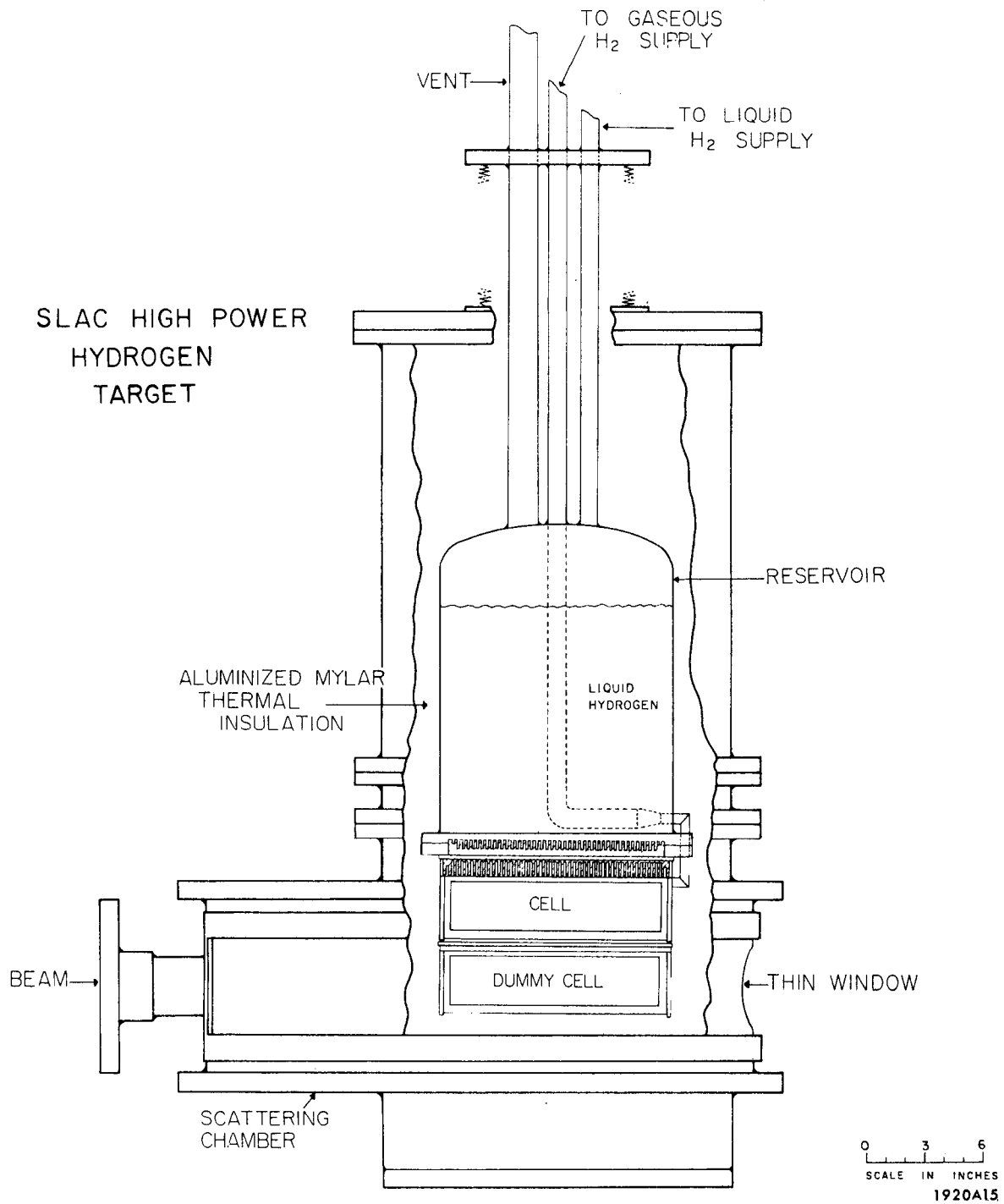
FIG. 16: Liquid Deuterium condensation target.

below. The limiting factor in our resolution in both p and θ is the multiple scattering of the recoil deuteron as it passes out of the target. The gas target shown in Fig. 15 was used at low |t| where the effect is greatest to improve resolution. The scattering chamber was connected directly to the spectrometer vacuum chamber and rotated about the target cells. The recoil deuteron had to pass through only the deuterium gas in the target, a 10mil mylar window in the side of the target cell, and a similar window at the top of the spectrometer vacuum chamber to reach the scintillation counters. Since the range of the deuterons is quite short at low |t| the first two trigger counters were only 1/32" thick. At larger |t| the effects were not critical and the improved rate afforded by the denser LD_2 target was needed (see Fig. 16).

The electronics is diagrammed in Fig. 17. Each scintillation counter was clipped with a 2nsec cable to reduce dead time effects. The signals were attenuated a variable amount and passed through a fixed 250m volt discriminator. All coincidence units shown are of standard Chronetics type with switchable inputs. Depending on the |t| value the appropriate coincidence was made to select the trigger signal. Table 7 lists the signals used. If desired, the lucite threshold Cerenkov counter could be put in veto. This signal was produced by adding the signals
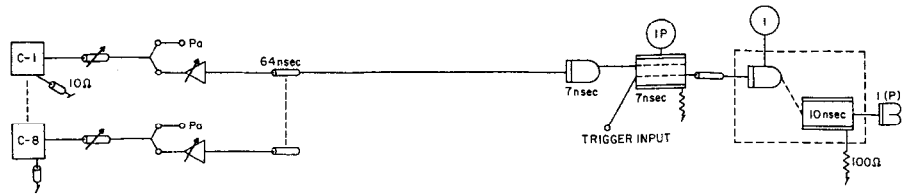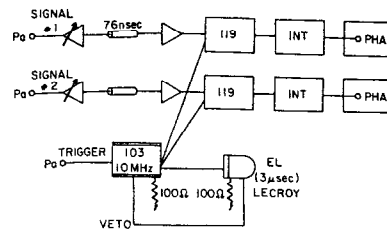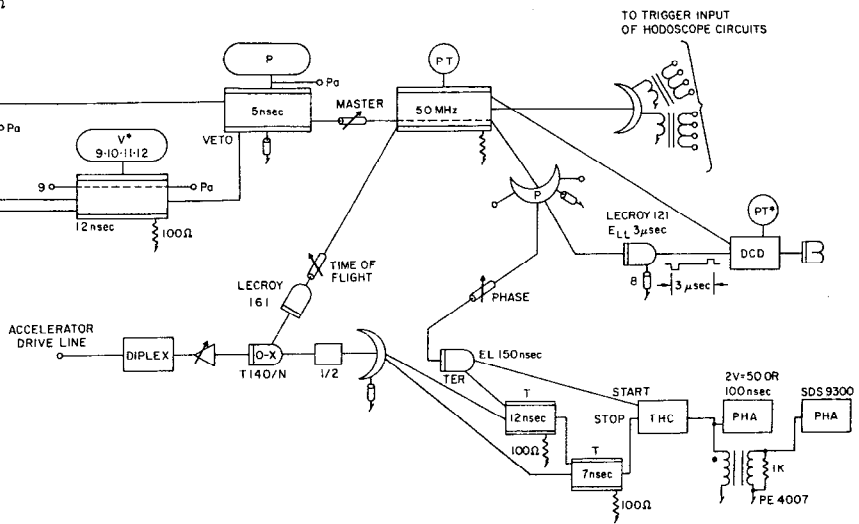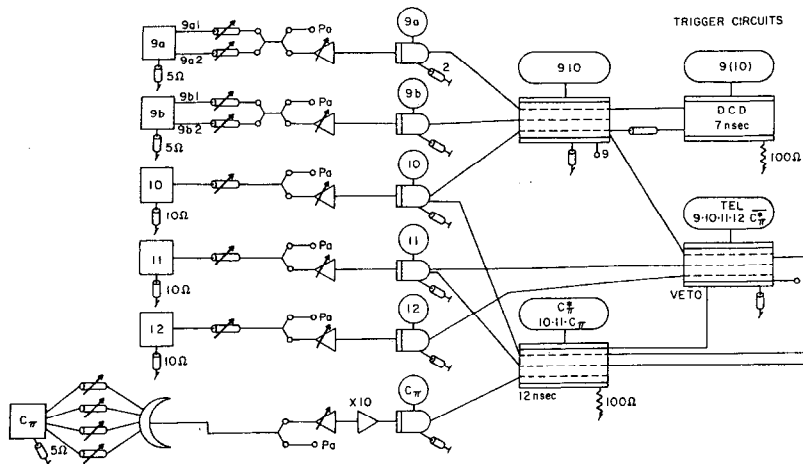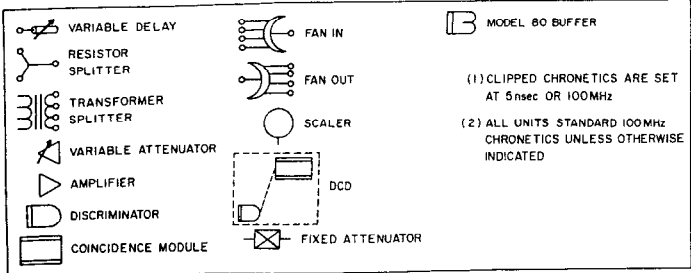
FIG. 17: Electronics diagram.

from the four phototubes attached to the lucite block. One could also place any of the trigger counters in veto to reject particles with too great a range. The trigger signal was then fed to the start input of a linear time-to-height converter. The time-of-flight synch signal from the accelerator was fed to a zero crossing circuit to provide stop pulses to the time-to-height converter and to trigger the window. The output of the time-to-height converter could then be analyzed by a standard pulse height analyzer to display the time-of-flight spectrum. Toggles were used to sample the spectrum at a maximum rate of 1/accelerator beam pulse to match the rep rate of the P.H.A. This output from the zero crossing circuit was input to a variable width pulse shaper producing a time-of-flight window which was put in coincidence with the trigger signal. The resulting coincidence was then used to gate the hodoscope counter signals into 100mhz scalars.

All beam monitors and scalars were started and stopped synchronously by an on-line SDS9300 computer. This computer has a basic cycle time of 2μsec and a 32K memory composed of 24 bit words. In addition, a high speed drum with a 2 million word capacity was used. A more detailed description of the computer can be found in Dave Gustavson's Thesis(29). The computer recorded the value of all these instruments at the end of each data taking run

for later analysis. A number of counting rates were sampled by the computer on an accelerator beam pulse by pulse basis. This provided additional scaling capabilities where the rates were low enough. The computer also aided us in performing the necessary real-time calculations and in making checks on the apparatus. Furthermore, the computer was able to present the raw data in a number of meaningful ways enabling us to detect malfunctions in the apparatus and human errors quickly. Of course, all data where such malfunctions or errors were detected are excluded from the analysis.

III. DATA ANALYSIS

Since the mass distribution of the ρ^0 is in some sense known and the background unknown, the procedure for extracting the cross sections emphasized projecting out the known shape from the data and to let the background be constrained only by mild smoothness and reasonableness criteria. Therefore, each excitation curve (Fig. 12b) was fit to the following form:

$$R(p,\theta,E_0) = A + B(\theta) + C\, M_x^2(p,\theta,E_0) + D\, M_x^4(p,\theta,E_0) + E\, f(p,\theta,E_0)$$

where the values of C and D were restricted to zero in the non-physical region ($M_x^2 < 0$). The function $f(p,\theta,E_0)$ is the representation of the ρ^0 contribution which we want to

measure and is given by:

$$f(p, \theta, E_o) = \int_0^{E_o} B(k, E_o) \, D \, (M_x(p, \theta, k)) \, \frac{1}{(p\cos\theta - T)} \, s(\frac{k}{E_o}) \, \frac{1}{\sin\theta} \, dk$$

where $B(k, E_o)$ is the bremsstrahlung distribution

$k \, dn(k)/dk$, $D(M_x)$ is the ρ^o mass distribution and $s(k/E_o)$

is a factor representing the s-dependence of $d\sigma/dt$. The

factor $1/\sin\theta$ is necessary due to the fact that $\Delta\phi/4\pi$

changes as the spectrometer rotates about the target. The

Jacobian transformation and the target length each have a

factor of $\sin\theta$ which cancel each other. Then E can be seen

to be $\propto d\sigma/dt(s,t)$. All other terms represent background.

It immediately became clear that we could set $s(k/E_o)=1$

without increasing our errors. This follows from internal

consistency with our final results. s-channel resonance

effects at low energy are unimportant due to the kinematic

effect on the spectrometer acceptance (see Fig. 14).

$B(k/E_o)$ was calculated using a computer program

supplied by R. A. Early(17). In the case where the

electrons passed through the target, the output of the

program can be taken directly along with the following

relation:

$$\frac{dW_\gamma}{dt} = E_o \, n_e \, (\frac{r}{r_o})$$

where n_e is the number of electrons/sec and r/r_o is the thickness of the radiator in radiation lengths. An additional correction was necessary to account for electroproduction.

In the case where the electrons were not allowed to pass through the target and the SEQ was used to measure photon beam power directly, the calculated spectrum was normalized according to:

$$\int_o^{E_o} B(k,E_o)dk = 1$$

The hydrogen experiment had been analyzed with the idea of being as shape independent as possible. For formalizing the shape one could emphasize contributions from the peak of the distribution and de-emphasize contributions from the tails. $D(M_x)$ was chosen to be exactly equivalent to the distribution used in the hydrogen analysis and is given by a Jackson-Selleri Breit-Wigner expression:

$$D(M_x) = \frac{2M_x M_o}{\pi} \frac{\Gamma(M_x)}{(M_x^2 - M_o^2)^2 + M_o^2 \Gamma^2(M_x)} \qquad (15)$$

where

$$\Gamma(M_x) = \Gamma_o \left(\frac{q}{q_o}\right)^{3/2} \frac{2}{1 + (q/q_o)^2} \qquad (16)$$

The last factor in Eq. 16 is a weak convergence factor
chosen by Selleri to provide a finite normalization. The
values of M_o and Γ_o were set to correspond with the
hydrogen experiment.

$$M_o = 765 \text{ MeV}$$

$$\Gamma_o = 125 \text{ MeV}$$

This expression was integrated numerically and normalized
so that:

$$\int_o^\infty D(M_x) \, dM_x = 1$$

Other shapes can be used and yield different values for
the cross section. The dependence of the cross section on
the shape is the same in the two experiments however and
doesn't effect the value of σ_T. Fig. 18 shows three
possible ρ mass distributions. The dashed line is taken
from Asbury et al.(DESY) obtained with a π pair
spectrometer. The dotted line is taken from
Bingham et al.(SLAC) obtained with a hydrogen bubble
chamber. The solid line is the relativistic BW used in a
previous experiment(4) to analyze the hydrogen
photoproduction data. A fourth shape is available from
McClellan et al.(CORNELL) which is for our purposes
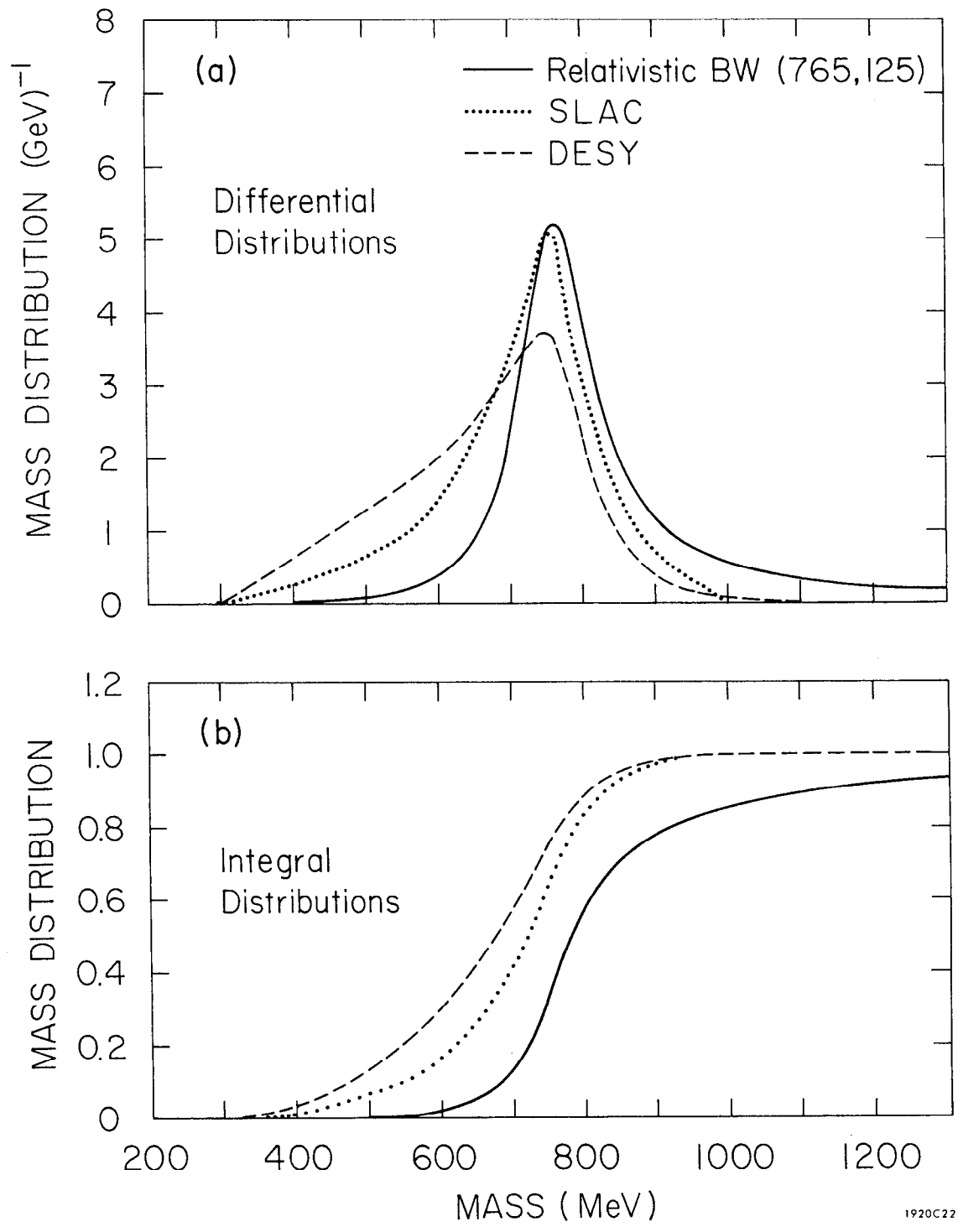
FIG. 18: ρ^0 mass distribution.

equivalent to the SLAC shape.

Our data systematically preferred the SLAC-CORNELL shape over the Jackson BW by about 1 standard deviation in x^2. The best description of this shape is given by Söding(45). This effect was particularly noticeable at low $|t|$. This result is consistent with the hydrogen analysis at low $|t|$. At high $|t|$ we noticed no preference for the Jackson as was found in the hydrogen analysis. The differences in cross section among these curves can be seen to depend on two things: the median mass value and the FWHM width of the distribution. If one adjusts the mass scale on each of these curves so that the median masses occur in the same place, the cross sections for all three curves agree to $< 5\%$. However as they are drawn, the DESY curve produces a 20% larger cross section than does the BW on the average. Since this represents a change in mass of 15% the sensitivity to the median mass is 4/3. By adjusting the width of the BW one can determine the sensitivity to the width (Γ) to be 1/2. In order to compare our cross sections to the hydrogen cross section we chose the canonical BW form having M_o = 765 MeV and a width Γ_o = 125 MeV. If you like a different ρ shape, you can correct our reported cross sections to conform to it according to the above discussion.

To take into account effects of multiple scattering,

$f(p,\theta,E_0)$ was folded into a Gaussian distribution in θ:

$$f(p,\theta,E_0) \leftarrow \int_0^\infty A\exp\left[\frac{(\theta-\theta')^2}{\langle\theta\rangle^2}\right] f(p,\theta',E_0)\, d\theta'$$

where A is chosen such that

$$\int_0^\infty A\exp\left[\frac{(\theta-\theta')^2}{\langle\theta\rangle^2}\right] d\theta' = 1$$

$\langle\theta\rangle^2$ was calculated from a gaussian approximation to the theoretical form of Bethe(8).

The particular form of the background functions was chosen to correspond with that used in the hydrogen analysis. The backgrounds that are unique to deuterium can be seen to take a form similar to multi-pion production and are indistinguishable from it. Therefore, we feel the background assumptions are compatible for the two experiments.

Fig. 19 shows the hydrogen data from Anderson et al.(4) used to extract $\sigma_T(\rho N)$ and $d\sigma/dt(\rho N)$ from our data. The solid lines are the quark model fit described in that paper. We assumed the fit to be correct and calculated $d\sigma/dt(\gamma p \to \rho^0 p)$ from it. To check this assumption, we did a least squares fit to the hydrogen data to a form:

$$\frac{d\sigma}{dt} = Ae^{Bt+Ct^2}$$
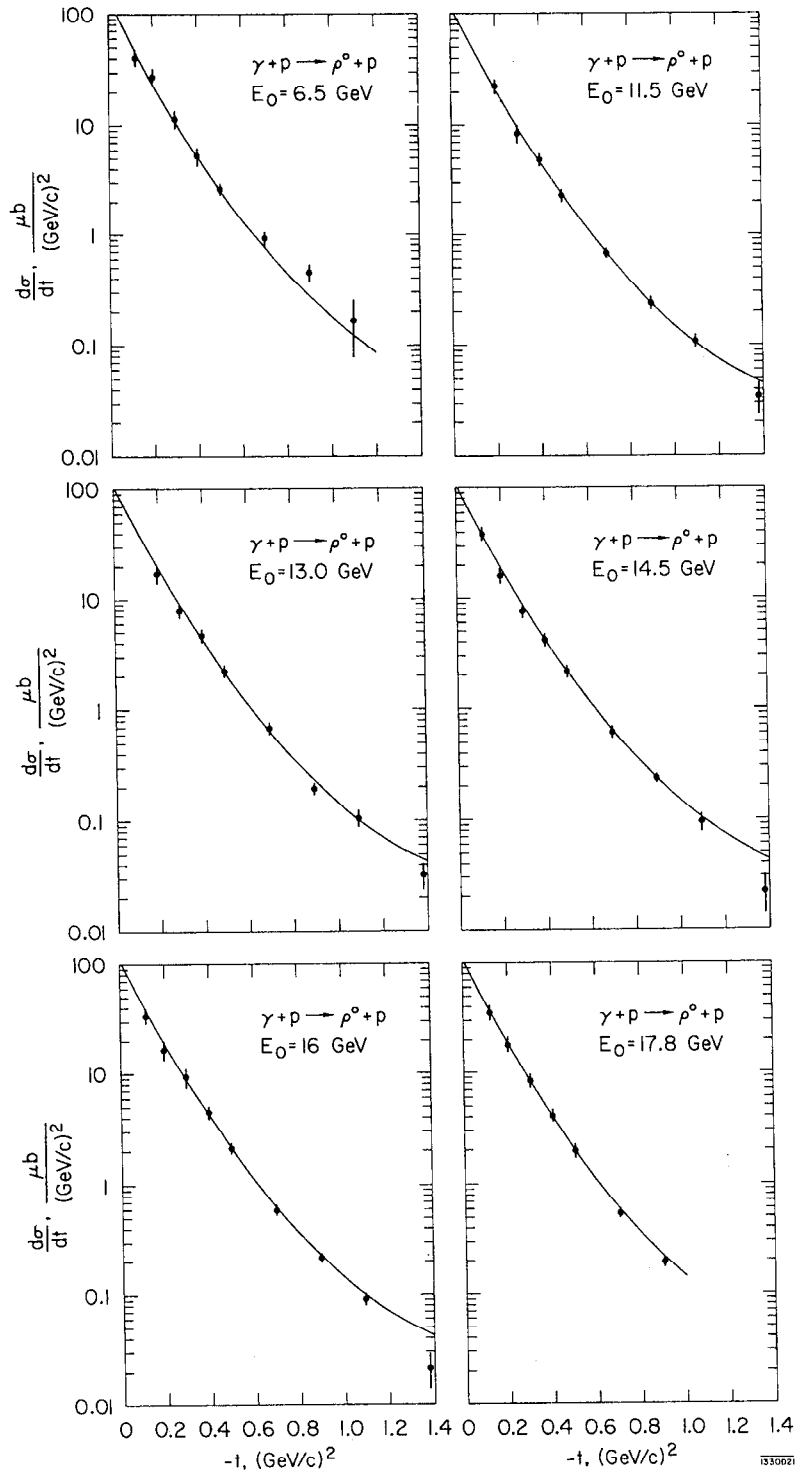
FIG. 19: $\gamma + p \rightarrow \rho^0 + p$ cross sections.

Using this curve changed the value for σ_T by 2%. In either case, Eq. 7 was evaluated using the hydrogen data assuming the t-dependence of the elastic cross section to be identical and leaving σ_T a free parameter. σ_T was determined from a least squares fit to our data for $|t| \geqslant .7(GeV/c)^2$.

The form factors were computed directly from an analytic form of Humberston which reproduces the ground state wave functions of Hamada and Johnson(30). The integrals K_0 and K_2 were computed by assuming an exponential behavior for the cross sections and again assuming identical t-dependence, to wit:

$$\frac{d\sigma}{dt}(\gamma\rho) \propto \frac{d\sigma}{dt}(\rho N) \propto e^{-Aq^2} \sim e^{At} \qquad (17)$$

Table 1-3 list the values of K_0 and K_2 one obtains in the manner. The data in these tables were calculated assuming $q^2 = -t$. This assumption was not made in the final determination and hence the values are somewhat different from our final values. Nevertheless the dependence on A can be seen clearly. K_0 varies slowly with A while K_2 varies somewhat faster. The value of A was determined from the hydrogen data by fitting to the form of Eq. 17 for $|t| \leqslant 0.6(GeV/c)^2$ and found to be $6 \pm .5(GeV/c)^{-2}$. This made K_0 uncertain by $\pm$ 1% and K_2 by

TABLE 1

FORM FACTOR INTEGRALS
as a function of leading coefficient
for incident photon energy of 6 GeV

A	$K_0(A) \, mb^{-1}$	$K_2(A) \, mb^{-1}$
.5	.160	.176
1.0	.167	.160
1.5	.173	.144
2.0	.177	.131
2.5	.179	.119
3.0	.180	.109
3.5	.180	.100
4.0	.179	.932
4.5	.178	.866
5.0	.177	.808
5.5	.175	.756
6.0	.173	.710
6.5	.171	.669
7.0	.168	.631
7.5	.166	.598
8.0	.164	.567
8.5	.162	.539
9.0	.160	513
9.5	.157	.489
10.0	.155	.467

TABLE 2

FORM FACTOR INTEGRALS
as a function of leading coefficient
for incident photon energy of 12 GeV

A	$K_0(A)mb^{-1}$	$K_2(A)mb^{-1}$
.5	.173	.176
1.0	.180	.160
1.5	.186	.144
2.0	.190	.131
2.5	.192	.119
3.0	.193	.109
3.5	.193	.100
4.0	.192	.933
4.5	.191	.868
5.0	.189	.809
5.5	.188	.758
6.0	.186	.712
6.5	.184	.671
7.0	.181	.633
7.5	.179	.599
8.0	.177	.569
8.5	.175	.541
9.0	.172	.515
9.5	.170	.491
10.0	.168	.469

TABLE 3

FORM FACTOR INTEGRALS
as a function of leading coefficient
for incident photon energy of 18 GeV

A	$K_0(A) mb^{-1}$	$K_2(A) mb^{-1}$
.5	.175	.176
1.0	.183	.160
1.5	.189	.144
2.0	.193	.131
2.5	.195	.119
3.0	.196	.109
3.5	.196	.100
4.0	.195	.934
4.5	.194	.868
5.0	.192	.810
5.5	.191	.758
6.0	.189	.712
6.5	.186	.671
7.0	.184	.633
7.5	.182	.600
8.0	.180	.569
8.5	.177	.541
9.0	.175	.515
9.5	.173	.491
10.0	.171	.469

TABLE 4

SPECTROMETER PARAMETERS

Maximum momentum	1.60 GeV/c
Maximum field	21.0kG
Maximum current	2840A
Voltage at 21.0 kG	440 V
Maximum power	1.25 MW
Momentum dispersion	4.19cm per % momentum
Momentum resolution	$\pm$ 0.08%
Momentum acceptance	$\pm$ 5%
Horizontal angular acceptance*	$\pm$ 17mrad
Vertical angular acceptance	$\pm$ 60mrad
Solid angle	4.1 msterad
Angular dispersion	0.823cm/mrad
Angular resolution $\Delta\theta$	$\pm$ 0.37mrad
Target length	20cm
Radius of central ray	254cm
Focal lengths	254cm
Field index	η=0,90° arc
Entrance β †	11.5
Central β	-10.0
Exit β	10.0
Entrance face angle	28°
Exit face angle	22°
Number of turns	144
Average length of each turn	9.1m
Number of turns/water circuit	3
Conductor size	1.59X1.80cm
Diameter of hole in conductors	0.95cm
Conductor area	2.13cm^2
Weight of magnet iron	78 ton
Weight of copper conductor	1.8 ton
Weight of shielding	205 ton
Weight of carriage	15 ton

*Bend plane is vertical.
† The three β sections each are 50.8cm in length.

$\pm$ 5%. The final values were K_0 = .188mb^{-1}, .190mb^{-1}, .192mb^{-1} for E_0 = 6, 12, and 18 GeV respectively and K_2 = .72mb^{-1} for all three energies.

IV.   RESULTS AND DISCUSSION

The measured cross sections for γ + d $\rightarrow \rho^0$ + d are shown in Fig. 20 and listed in Table 5. The solid line in Fig. 20 represents the published fit to the data using the Glauber theory. This fit does not include a relativistic extension to the Glauber theory proposed by Faldt(18). This correction is included in the final results quoted in Table 6, however. The effect of this correction is to raise σ_T by 3%. The data from γ + p $\rightarrow \rho^0$ + p were used along with the assumption that the t-dependence of both processes are identical. The ratio of real to imaginary part of the $\rho^0 N$ scattering amplitude was input using the values shown in Table 6. The fit was allowed to optimize only those data points from $|t|$ = 0.7(GeV/c)^2 and above to minimize theoretical uncertainties in applying the Glauber theory. The result of the fit was then evaluated over the entire range to provide the curve shown. The curve fits well except in the interference region around $|t|$ = 0.4(GeV/c)^2. In this region the real part of the scattering amplitude as well as the D-state wave function have important effects(31). The values of a in Table 6 were taken from the dispersion relation result on Compton

-55-
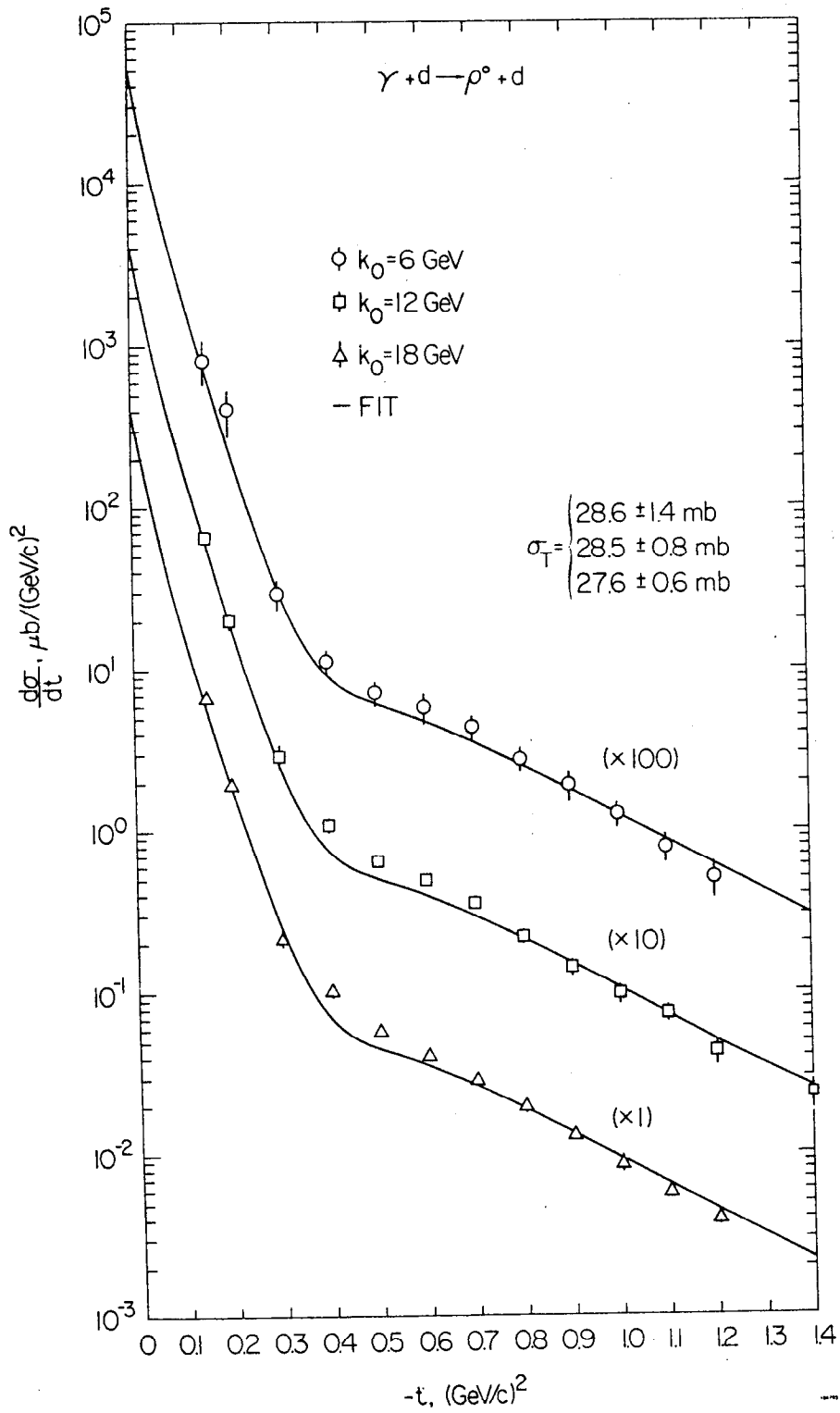
FIG. 20: Differential cross section.

TABLE 5

Differential Cross Sections for $\gamma + d \rightarrow \rho^0 + d$

t	$\frac{d\sigma}{dt}$ for $k_o = 6$ GeV $(cm^c/GeV)^2$	$\frac{d\sigma}{dt}$ for $k_o = 12$ GeV	$\frac{d\sigma}{dt}$ for $k_o = 18$ GeV
0.15	$(8.25 \pm 2.5) \times 10^{-30}$	$(6.59 \pm .41) \times 10^{-30}$	$(6.62 \pm .38) \times 10^{-30}$
0.2	$(4.08 \pm 1.3) \times 10^{-30}$	$(2.02 \pm .23) \times 10^{-30}$	$(1.94 \pm .11) \times 10^{-30}$
0.3	$(2.94 \pm .60) \times 10^{-31}$	$(2.95 \pm .47) \times 10^{-31}$	$(2.14 \pm .29) \times 10^{-31}$
0.4	$(1.13 \pm .20) \times 10^{-31}$	$(1.09 \pm .11) \times 10^{-31}$	$(1.04 \pm .10) \times 10^{-31}$
0.5	$(7.15 \pm 1.29) \times 10^{-32}$	$(6.50 \pm .52) \times 10^{-32}$	$(5.97 \pm .54) \times 10^{-32}$
0.6	$(5.81 \pm 1.28) \times 10^{-32}$	$(4.92 \pm .39) \times 10^{-32}$	$(4.16 \pm .32) \times 10^{-32}$
0.7	$(4.40 \pm .75) \times 10^{-32}$	$(3.57 \pm .29) \times 10^{-32}$	$(2.95 \pm .21) \times 10^{-32}$
0.8	$(2.78 \pm .47) \times 10^{-32}$	$(2.20 \pm .22) \times 10^{-32}$	$(2.01 \pm .11) \times 10^{-32}$
0.9	$(1.90 \pm .40) \times 10^{-32}$	$(1.41 \pm .16) \times 10^{-32}$	$(1.32 \pm .11) \times 10^{-32}$
1.0	$(1.25 \pm .21) \times 10^{-32}$	$(9.73 \pm 1.36) \times 10^{-33}$	$(8.7 \pm 1.1) \times 10^{-33}$
1.1	$(7.80 \pm 1.56) \times 10^{-33}$	$(7.39 \pm .81) \times 10^{-33}$	$(5.88 \pm .59) \times 10^{-33}$
1.2	$(4.98 \pm 1.25) \times 10^{-33}$	$(4.26 \pm .72) \times 10^{-33}$	$(4.05 \pm .45) \times 10^{-33}$
1.4		$(2.34 \pm .47) \times 10^{-33}$	

TABLE 6

Results of Glauber Analysis

k_o(GeV)	αp	σ_T(mb)	$\gamma_\rho^2/4\pi$
6	$-.27$	29.6 ± 1.4	$.66 \pm .06$
12	$-.22$	$29.4 \pm .8$	$.75 \pm .04$
18	$-.16$	$28.5 \pm .6$	$.75 \pm .03$

scattering of Damashek and Gilman(15). We have further
assumed the a's to be equal for the two processes. While
the Compton result is probably good to about 10% the
validity of our assumption is questionable. It is possible
to construct Feynman diagrams which allow for the phases to
be different but still preserve Vector Dominance
(see Fig. 7). Fortunately, our result for σ_T is quite
independent of this problem since the interference term is
negligible for $|t| \geqslant 0.7(\text{GeV}/c)^2$. The D-state
probability of the deuteron is taken to be 7% from the wave
functions of Hamada and Johnson.

The errors quoted on the $\gamma + d \rightarrow \rho^0 + d$ cross sections
are part statistical and part systematic. The incoherent
background under the ρ^0 step was estimated by studying the
behavior of our fits to be uncertain by ± 30%. It should
be noted that the analysis is based on very restrictive
theoretical assumption on the ρ^0 mass distribution. While
this tends to make the meaning of our measured cross
sections less intuitive, it affords a high degree of
reliability in comparing this experiment with the hydrogen
experiment hence in determination of σ_T. Unfortunately,
the determination of $\gamma_\rho^2/4\pi$ is subject directly to all the
experimental errors.

The data were corrected for detection inefficiency
losses due to nuclear absorption in the material in the

TABLE 7

Coincidence Required for
Deuteron Trigger at Various $|t|$

$|t|$	Coincidence
0.15	$9a \cdot 9b \cdot \overline{9a \cdot 9b \cdot 10}$
0.2	$9a \cdot 9b \cdot 10$
0.3	$9a \cdot 9b \cdot T$
0.4-1.4	$9 \cdot 10 \cdot T$

path of the recoil deuterons, for loss of photons in the
target, and for changes in spectrometer acceptance due to
energy losses in the target deuterium. The absorption
corrections were not well understood and contributed as
much as 10% to the systematic error at low $|t|$. Again, the
losses are on the order of 2% in the double scattering
region and did not effect the determination of σ_T. This is
particularly important since this is a point of difference
between the two experiments. The spectrometer acceptance
is known to 3% and the calibration of the beam monitors to
2%.

There are several approximations inherent in the
Glauber theory. For example, the fermi motion of the
nucleons has been neglected. Furthermore, the theory is
strictly non-relativistic. However this approach has been
shown to be valid for the closely related process
$\pi^- + d \rightarrow \pi^- + d$(21,25). Here we have elastic scattering on
both nucleons with the results that: $f_e(q) \equiv f_\rho(q)$ in
Eq. 6. Furthermore, the elastic cross section is known to
high precision(23). Consequently Eq. 7 is greatly
simplified for this process and yields an exact predictive
result in which there are no free parameters. Recently,
the $\pi^- + d \rightarrow \pi^- + d$ cross section has been measured to high
precision(21) in excellent agreement with the Glauber
prediction.

In applying the theory to $\gamma + d \rightarrow \rho^0 + d$ it must be noted that the photoproduction process is not elastic. We have also not discussed the possibility that the state which propogates from one nucleon to the other in the double scattering case is something other than a ρ^0. If there were significant contributions from inelastic states, they would tend to require a large momentum transfer. Since the deuteron form factors vanish rapidly, we have neglected these states. The consequences of ignoring these effects are thought to be small but numerous and may tend to cancel somewhat(41). Therefore, rather than attempt to correct for any particular flaw and inject a bias we made no corrections for difficiencies in the Glauber theory as we applied it other than the relativistic extension of Faldt(18) given below:

$$\frac{d\sigma}{dt} \quad \frac{1}{1 + |t|/16M_n^2} \quad \frac{d\sigma}{dt} \quad \text{(Glauber)}$$

The total cross sections are shown in Table 7 along with the derived values of $\gamma_\rho^2/4\pi$. σ_T falls slightly with energy as one would expect.

$\gamma_\rho^2/4\pi$ is consistent with being independent of energy to good precision. This statement is more precise than the quoted absolute value of $\gamma_\rho^2/4\pi$ since presumably the unknown systematic errors in normalization do not vary with energy.

As we can see by looking at an excitation curve
Fig. 12(b) our resolution is insufficient to resolve the
ω-photoproduction from that of the ρ^o. In actual fact we
measure the incoherent sum of the two processes. We assume
that the ω cross section is related to that of the ρ^o by:

$$9 \frac{d\sigma}{dt}(\gamma + p \rightarrow \omega + p) = \frac{d\sigma}{dt}(\gamma + p \rightarrow \rho^o + p) \qquad (18)$$

This result is predicted by SU(3) and ω-ϕ mixing theory.
The experimental validity of this statement has been
established to fair accuracy(16). We now rely on a well
known quark model prediction:

$$\frac{d\sigma}{dt}(\omega + N \rightarrow \omega + N) = \frac{d\sigma}{dt}(\rho^o + N \rightarrow \rho^o + N)$$

$$= \left\{ \frac{1}{2}\left[\frac{d\sigma}{dt}(\pi^+ + p \rightarrow \pi^+ + p)\right]^{1/2} + \frac{1}{2}\left[\frac{d\sigma}{dt}(\pi^- + p \rightarrow \pi^- + p)\right]^{1/2} \right\}^2 \qquad (19)$$

The first half of this statement Eq. 19 has been implicitly
assumed in our previous statement above in Eq. 18. Now if
we apply the Glauber theory to the ω as we have to the ρ^o
we see:

$$9 \frac{d\sigma}{dt}(\gamma + d \rightarrow \omega + d) = \frac{d\sigma}{dt}(\gamma + d \rightarrow \rho^o + d) \qquad (20)$$

Implicit in this statement is an assumption that the ω is 100% diffractive.

Following our earlier experiment we have used the above reasoning to infer that the ρ^o cross section is just 90% of the total we observe in each experiment. Again, if this number is not correct the value of σ_T is unaffected while $\gamma_\rho^2/4\pi$ is directly effected. It would be particularly unnerving if the t-dependence of the two cross sections differed. Unfortunately, ω cross sections are not well known and the validity of Eq. 20 will have to be treated as somewhat of an assumption. Certainly if Vector Dominance is correct Eq. 20 is true.

There are also other processes which can cloud the issue. Consider the process shown in Fig. 21 where the photon produces a pion-pair each of which scatters on his own nucleon in such a way that the end result looks like a ρ^o. After careful study(28), it appears as though this process enters smoothly at the two-pion threshold and thus is interpreted by our fitting program as background.

Fig. 22 shows our extracted $\rho^o N$ differential cross sections which were obtained simply by solving the quadratic Glauber relation (eq. 7) point by point. No assumptions were made as to the t-dependence of the $\rho^o N$ cross section except the assumptions used in evaluation of the K_0 and K_2 integrals. The extraction was made only in
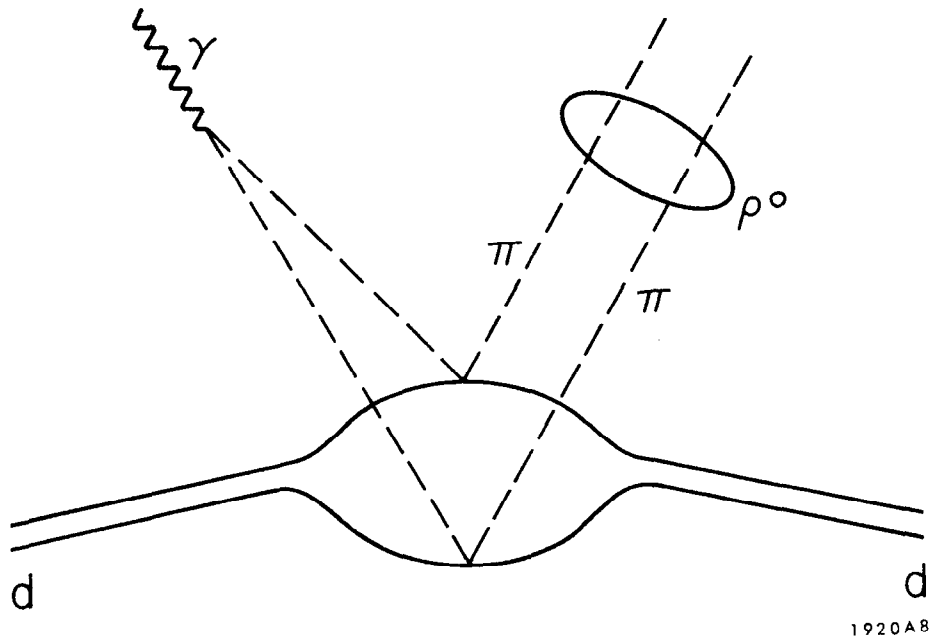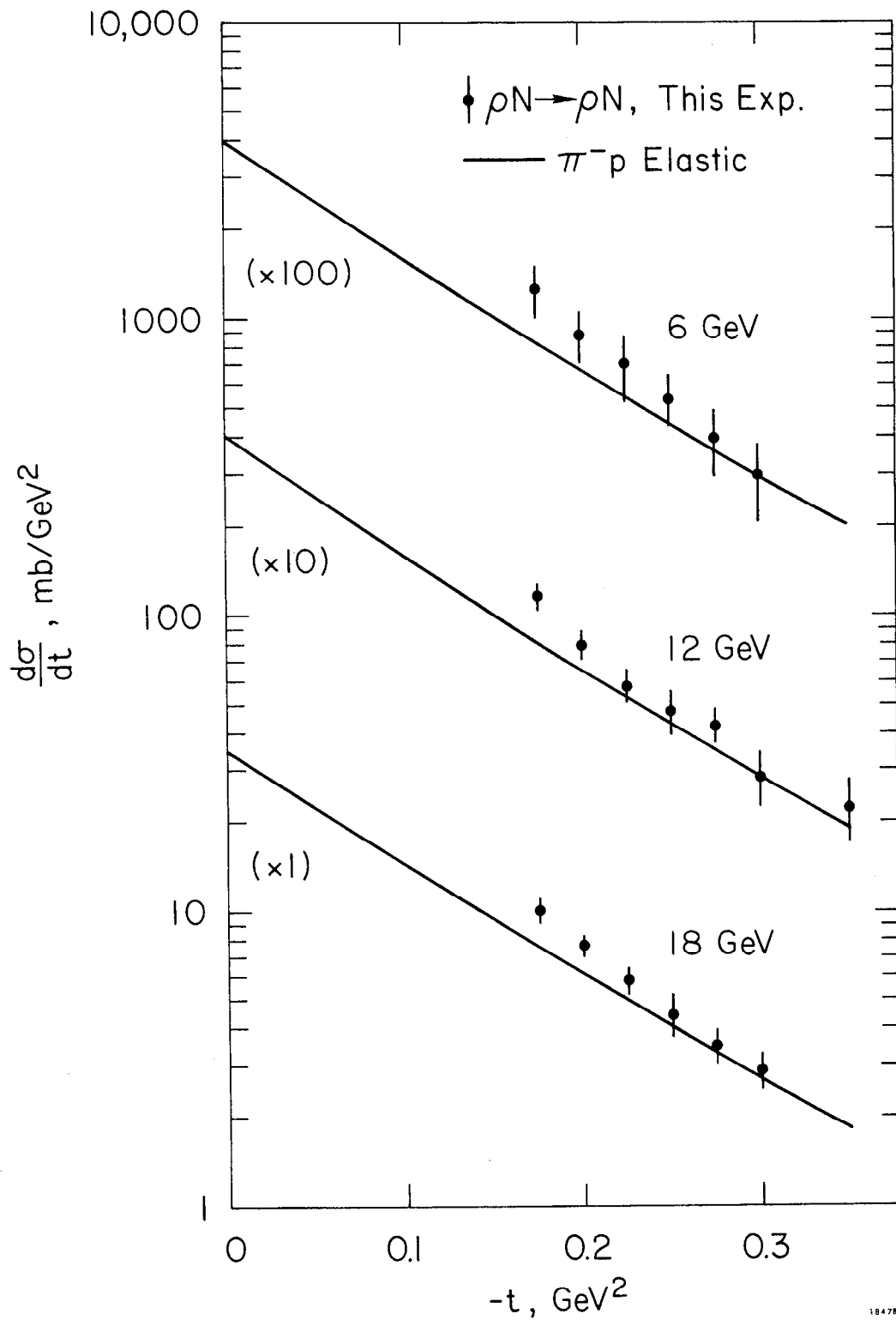
FIG. 21: π pair scattering diagram.

FIG. 22: Extracted differential cross section.

the double scattering region due to the same kind of errors mentioned in connection with σ_T. The solid lines are $d\sigma/dt(\pi^- + p \to \pi^- + p)$ from K. J. Foley et al.(23). Our results are very close to the quark model prediction but are always high. Furthermore, our value of σ_T is significantly higher than the corresponding quark model prediction.

We have assumed that the amplitude for photoproduction at these energies is entirely transverse. Experiments at Cornell where the ρ^o laboratory polarizations have been measured justify this assumption(7,37). We have also assumed no isovector exchange contribution to the hydrogen amplitude also supported by Cornell experiments(37).

The essential feature of this experiment is that the results for σ_T are quite reliable. It is therefore possible to use the newly determined value of σ_T to improve measurements of $\gamma_\rho^2/4\pi$ made in other experiments. If one would re-analyze lower energy coherent photoproduction experiments on nuclei with the objective of determining the phase of the ρN amplitude given the total cross section, one could then derive a much better value for $\gamma_\rho^2/4\pi$. Figure 23 shows one way to do this taken from Göttfried(20). The graph indicates that the ratio of real-to-imaginary parts of the ρN amplitude is about -.2 consistent with Compton. One can also see clearly the
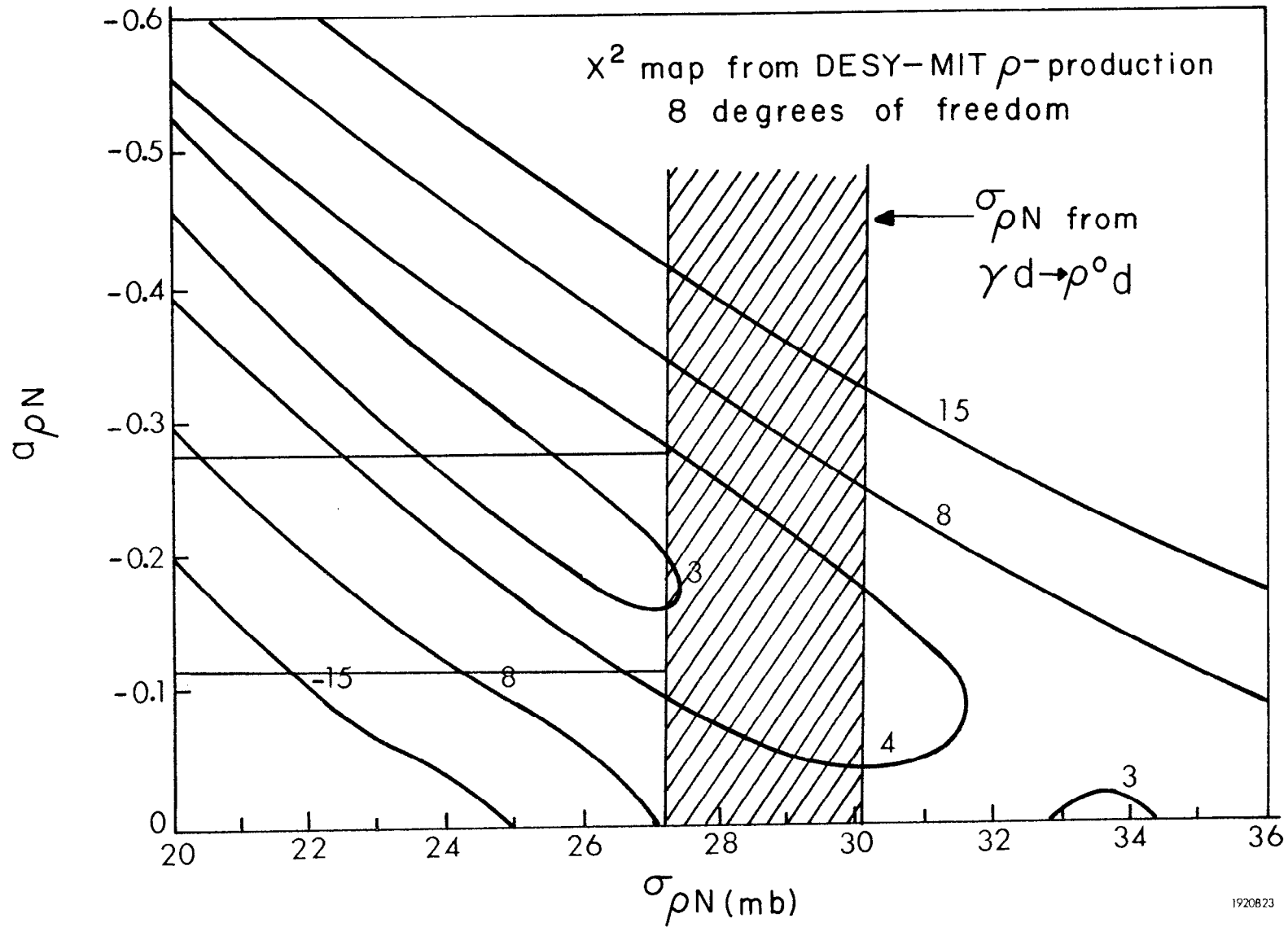
FIG. 23: Comparison with heavy nucleii.

fundamental ambiguity inherent in nuclear photoproduction experiments.

The value of $\gamma_\rho^2/4\pi$ from storage ring experiments appears now to be approximately .65(36). One cannot say whether this is something fundamental (i.e. γ_ρ^2 independent of q^2), or is just an accident.

Our value can be compared directly to the value obtained from total photoabsorption cross sections in the following way. According to Vector Dominance with saturation of the electromagnetic current we have:

$$\sigma_{\gamma N}(E) = \frac{\alpha}{4}\left(\frac{4\pi}{\gamma_\rho^2}\right)\sigma_{\rho N}(E) + \text{negligible terms} \tag{21}$$

At 12 GeV we have $\sigma_{\rho N} = 29.4 \pm .8$mb and from Caldwell et al.(13) $\sigma_{\gamma N} = 114.0 \pm 2.8\mu$b. This would give:

$$\frac{\gamma_\rho^2}{4\pi} = \frac{\alpha}{4}\frac{\sigma_{\rho N}}{\sigma_{\gamma N}} = \frac{1}{4(137)}\frac{29.4}{.114} = .47 + .03$$

This determination is quite precise and in direct theoretical contradiction with results for γ_ρ^2 based on photoproduction. Firstly, we can speculate that the background and resonant ρ^o events have not been clearly separated. In order for this to be correct, our determination of the photoproduction cross sections would have to change by a factor of 2/3 which is very unlikely.

-69-

Secondly, we can assume that Vector Dominance is correct in principle but that there is another or are several other particles of high mass which contribute in significant amounts to the electromagnetic current. Thirdly, we can surmise the existence of a continuum of states which add up to produce the needed contribution. These states would be very difficult to detect as they would exhibit no resonance behavior. Lastly, one can conclude that the photon can couple directly to hadrons without the necessity of an intermediate vector meson state. The results of recent colliding beam experiments(6) suggest this is indeed the case. This follows since the cross section for π pair production as well as other strong cross sections are much too large to be accounted for by Vector Dominance considerations.

It would seem therefore, that Vector Dominance contributes much to our understanding of photon-hadron interactions at $q^2 \sim 0$ but cannot be taken as a completely precise theory.

REFERENCES

1. H. Alvensleben, _et al._, Phys. Rev. Letters $\underline{24}$, 786, (1970).

2. R. L. Anderson, Nuclear Inst. and Methods $\underline{65}$, 195 (1968).

3. R. L. Anderson, _et al._, Nuclear Inst. and Methods $\underline{66}$, 328 (1968).

4. R. L. Anderson, _et al._, Phys. Rev. $\underline{D1}$, 27 (1970).

5. J. G. Asbury, _et al._, Phys. Rev. Letters $\underline{20}$, 227 (1968).

6. B. Bartoli, _et al._, Nuovo Cimento $\underline{70A}$, 615 (1970).

7. H. J. Behrend, _et al._, Phys. Rev. Letters $\underline{24}$, 336 (1970).

8. H. Bethe, Phys. Rev. $\underline{89}$, 1256 (1953).

9. H. H. Bingham, _et al._, Phys. Rev. Letters $\underline{24}$, 955 (1970).

10. J. M. Blatt and V. F. Weisskopf, _Theoretical Nuclear Physics_ (John Wiley and Sons, Inc., New York, 1952).

11. F. Bradamante, _et al._, Physics Letters $\underline{31B}$, 87 (1970).

12. F. Bulos, _et al._, Phys. Rev. Letters $\underline{26}$, 149 (1971).

13. D. O. Caldwell, _et al._, Phys. Rev. Letters $\underline{23}$, 1356 (1969).

14. R. Dalitz and D. Yennie, Phys. Rev. $\underline{105}$, 1598 (1957).

15. M. Damashek and F. Gilman, Phys. Rev. $\underline{D1}$, 1319 (1970).

16. M. Davies et al., Phys. Letters $\underline{28B}$, 619 (1969).

17. R. A. Early, SLAC-TN-66-55 (Stanford Linear Accelerator Center, Stanford, California), (1967).

18. G. Faldt, Nuclear Phys. $\underline{B29}$, 16 (1971).

19. G. Galdt, Phys. Rev. $\underline{D2}$, 846 (1970).

20. K. Göttfried, (to be published).

21. M. Fellinger, et al., Phys. Rev. Letters $\underline{22}$, 1265 (1969).

22. G. E. Fischer and Y. Murata, Nuclear Inst. and Methods $\underline{78}$, 25 (1970).

23. K. H. Foley, et al., Phys. Rev. Letters $\underline{11}$, 425 (1963).

24. V. Franco and R. J. Glauber, Phys. Rev. $\underline{142}$, 1195 (1966).

25. M. Giorgi, in Scole Internationale de la Physique des Particules Elementaires, Herceg-Novi, Yougoslavie (1969).

26. R. J. Glauber, Lectures in Theoretical Physics, Vol. I, 315 (Interscience Publishers, Inc., 1959).

27. J. Grant and B. H. Wiik (in preparation).

28. J. F. Gunion and R. Blankenbecler, SLAC-PUB-846 (1970) to be published.

29. D. Gustavson, Thesis, Stanford University (1968).

30. T. Hamada and I. D. Johnson, Nuclear Phys. $\underline{34}$, 382 (1962). We used the analytic form computed by J. Humberston and quoted in Michael and Wilkin, Nuclear Phys. $\underline{B11}$, 99 (1969).

31. D. Harrington, Phys. Rev. Letters $\underline{21}$, 1496 (1968).

32. D. L. Kreinick, Thesis, California Institute of Technology (1970).

33. N. M. Kroll, et al., Phys. Rev. $\underline{157}$, 1376 (1967).

34. L. J. Lanzerotti, et al., Phys. Rev. $\underline{166}$, 1365 (1968).

35. K. Lassila, et al., Phys. Rev. $\underline{126}$, 881 (1962).

36. J. Lefrancois, (to be published).

37. G. McClellan, et al., Lectures in Theoretical Physics, $\underline{11-A}$, 47 (1969). (Cornell University, Ithaca, New York). Also Phys. Rev. Letters $\underline{25}$, 478 (1970).

38. H. Ogren, Thesis, Cornell University (1970).

39. F. Partovi, Ann. Phys. $\underline{27}$, 79 (1964).

40. F. M. Pipkin, in Proceedings of the 1967 International Symposium on Electron and Photon Interactions at High Energies, Stanford Linear Accelerator Center. (Clearinghouse for Federal Scientific and Technical Information, National Bureau of Standards, Springfield, Virginia).

41. J. Pumplin, Phys. Rev. $\underline{173}$, 1651 (1968).

42. J. J. Sakurai, in Proceedings of the International School of Physics for 1963. (Academic Press, New York and London 1963) p.41.

43. J. J. Sakurai, in Proceedings of the Fourth International Symposium on Electron and Photon Interactions at High Energies, Liverpool, England, 1969. (Daresbury Nuclear Physics Laboratory, Daresbury, Lancashire, England, 1970).

44. A. Silverman, in Proceedings of the Fourth International Symposium on Electron and Photon Interactions at High Energies, Liverpool, England 1969. (Daresbury Nuclear Physics Laboratory, Daresbury, Lancashire, England, 1970).

45. P. Söding, Phys. Letters 19, 702 (1966).